2015

Characteristics of von Willebrand Factor multiuser in blood clotting

Wenli Ouyang
Lehigh University

Characteristics of von Willebrand Factor multimer in blood clotting

Submitted by:

Wenli Ouyang

Presented to the Graduate and Research Committee

Of Lehigh University

In Candidacy for the Degree of

Doctor of Philosophy

in

Mechanical Engineering

Lehigh University

Certificate of Approval

Approved and recommended for acceptance as a dissertation in partial fulfillment of the requirements for the degree of Doctor of Philosophy.

_____

Date

_____

Dissertation Director

_____

Accepted Date

Committee Members:

_____

Name of Committee Chair

_____

Name of Committee Member

_____

Name of Committee Member

_____

Name of Committee Member

Acknowledgements

While my name appears in the front page of this dissertation, it will be a disrespectful mistake to not acknowledge the sensational and profound inputs from my peers, family and mentors have done in its creation. This is as much an achievement of their emotional and academic supports as it is my own work, and this I am incredible indebted to a great many people. It is worth pointing out some of the most important individuals that have given me the help and support over the past few years.

First and foremost, my parents deserve the most credits for help me to go through a lot of unbearable moments. Without their help emotionally and financially, I can't make it to this point. The most important and valuable lesson they taught me is that always possess the mentality to get things done – "do it now" and "you will have the capability to do it once you do it". I hope this dissertation stands as a testament to their incredible patience and support.

I also owe many thanks to my advisors. Prof. Alparslan Oztekin is a great mentor who gave me masterful guidance academically and one of the kindest professors I have ever met who care me so much personally. I am influenced by his energy, his interpersonal skills, and his dedication to his research. Prof. Edmund Webb III has provided excellent guidance in the context of statistical mechanics and coarse-grained modeling. Prof. Xiaohui Zhang has provided valuable help setting up atomic force spectroscopy to measure the parameters we need in our projects. It was under their guidance that I realize my immense interest in polymer science, and I was their encouragement that set me on my current trajectory.

Contents

List of Figures

Abstract

The von Willebrand Factor (vWF) is a large multimeric protein in the blood that aids in blood clotting. It activates the clotting cascade at a specific time and a specific place, which is one of the human body's masterpieces in targeted molecular manipulation. Hydrodynamic or shear force triggers conformational changes of vWF, by which its potency and reactivity are regulated. In this thesis, we take inspiration from novel findings in the vWF experiments, and aim to describe the behaviors observed in this process within the context of polymer science. By understanding this physical principle, we hope to harness nature's ability to help us develop targeted drug therapy, which is capable to deliver drug wherever and whenever needed.

After initial introduction of the blood clotting process, we first propose a novel bead-spring model in the presence of infinite medium. Contrary to the classic bead-spring model that each bead is connected by one type of spring, our model's beads are connected by finitely extensible nonlinear elastic (FENE) springs and Hookean springs consecutively. The motivation is that the A2 domain, which undergoes significant unfolding during single molecule stretching experiments, has been proven to be very flexible. Instead of modeling a monomer as one bead, more details inside each monomer and more complexity of vWF multimer has been captured by modeling vWF monomers as a highly flexible A2 domain with relatively very rigid domains on either side of A2. The A2 domain is modeled as a finitely extensible nonlinear elastic (FENE) spring capable of significant extension. At each end of the spring is a spherical bead to represent neighboring rigid domains. Adjacent monomers are connected by a tight harmonic spring

successively to form vWF multimers of desired length. In an effort to validate our mythology and generalize our results quantitatively, vWF multimers represented by this model have been probed to understand a single vWF multimer in both relaxation without flow scenarios and unfolding in response to shear flow circumstances.

After investigating flow-induced changes in vWF multimer conformation, we extend our research further to study adhesion of vWF multimer by incorporating a collagen-coated surface to the vWF model in the second section of this thesis. During the blood clotting process, vWF undergoes a counterintuitive adsorption process and here we begin to develop the fundamental model required to understand this process. Because the presence of a pure surface will create a non-monotonic lift force, which greatly facilitate the desorption behavior of vWF multimer even under highly attractive surface, we add another A3 domain and collagen interactions representing by reversible ligand-receptor-type bonds based on bell model kinetics. The bonding and debonding rate between vWF multimers and collagen-coated surface is determined by the energy landscape i.e. binding and unbinding energy of bell model, which are measured by force spectroscopy and were extracted using the Dudko-Hummer-Szabo model under different temperature. The no-slip bond that the tensile force has no influence on the bond is being used firstly to counteract the lift force induced desorption. The results show that the adhesion process is still impeded by bead-wall hydrodynamic interactions, which is different from the experimental observations. The final section of this paper will be focused on the dynamics of vWF multimers in complex geometries, especially in a slit.

Chapter 1 Introduction

1.1 Biopolymer manipulation inspired by blood clotting

In the past few decades, one of the major motivations in the study of polymer science has been the desire to capture the power to manipulate the behavior of biopolymers. [1] The advance in understanding of thermodynamics, kinetics, and polymer chain structure in the context of polymer science worked together to strengthen the biophysical techniques for the manipulation, which in return made possible a large number of significant breakthroughs in polymer science, such as Nobel Prize winning research as Watson and Crick's discovery of the double helix structure of DNA and an understanding of the functionality of proteins in muscles. [2] A typical biopolymer manipulation is "protein unfolding". Although protein comprise a subset of biopolymers, the importance of protein unfolding studies using molecule manipulation techniques deserves emphasis. One notable example is the study of the proteins titin (important in maintaining sarcomere structural integrity and generating passive force in muscle), and tenascin (an extracellular matrix protein thought to provide a rigid mechanical anchor that supports and guides migrating and rolling cells). Individual protein molecules are investigated by stretching out from end-to-end at various speeds, using several different biophysical manipulation techniques including AFM, optical trapping nanometry, and optical trapping techniques. [3–5] These types of studies lay the cornerstones for the energy landscapes of individual protein exploration, which may be directly measured covering both smaller and larger time scales. Another protein unfolding technique is implemented under an indirect way – through the presence of fluid flows. Hemostasis is a well-balanced process that prevents excessive blood loss after vascular injury involving a

complex interplay between a plethora of agonists and antagonists. [6] Under abnormal conditions however, platelet-rich thrombi can occlude the vascular lumen, often resulting in cardiovascular disease, which is still the leading cause of death in the developed world. A large adhesive, multimeric glycoprotein named after Dr. Erik von Willebrand, who described the hereditary bleeding disorder at first, is crucial in this process that maintain the delicate balance between thrombosis and hemostasis. [6] The functionality of von Willebrand Factor (vWF) is related to the unfolding of it in response to the presence of strong fluid flows. vWF is able to bind to both subendothelial structures in the injured vessel wall and circulating blood platelets by supporting the formation of a platelet-rich plug that will prevent bleeding and promote wound healing, only when the vWF unfolding is happened to some extent. [7,8] In this thesis we will be primarily focusing on the characteristic of vWF protein that lends itself to comprehensive study due to the simplicity of its hierarchical structure despite its complex array of associations and sequence. Furthermore, the principles that will be gained from this study will suggest paths for engineering molecular systems capable of achieving a specific response in the human body, e.g. targeted drug therapy.

1.2 Blood Clotting Process – Coagulation

The blood clotting process also named coagulation is one of the most complicated phenomena in human body by which blood changes from a liquid to a gel. [7] The mechanism of coagulation involves activation, adhesion, and aggregation of platelets and more. In the absence of injury, vWF doesn’t appear to interact circulating platelets. [9] However, damaged blood vessels makes the endothelial cells no longer form a barrier between the blood inside and the extracellular matrix. Collagens, constituting most parts

of the extracellular matrix, interact with vWF that results in the deposition of vWF on the damaged vessel wall under the influence of fluid flows. It also enables vWF to bind platelets with affinity sufficient to snare them from rapidly flowing blood and retains them at the site of injury. Interestingly, platelets have no measurable interaction with soluble vWF in the circulation, but adhere prompt to exposed immobilized vWF. [10] This localization of platelets to the extracellular matrix promotes collagen interaction with platelet glycoprotein VI. Binding of collagen to glycoprotein VI triggers a signaling cascade that results in activation of platelet integrins. Activated integrins mediate tight binding of platelets to extracellular matrix. Activated platelets release the contents of stored granules into the blood plasma, which in turn, activate additional platelets. The activated platelets change shape from spherical to stellate and aid in aggregation of adjacent platelets. These platelets then, along with more vWF molecules, form an initial gel structure known as a “plug”. [10]

1.3 Structure and Functionality of Von Willebrand Factor

von Willebrand Factor is one of the initial actuators in the blood clotting cascade, which is made by endothelial cells throughout the body. [7] Endothelial vWF is stored in Weibel-Palade bodies and secreted both to the lumen and the extracellular matrix upon stimulation. Once secreted into the plasma, circulating vWFs are in its ultra-large state and are the most active ones as they provide multiple interactive sites for ligand binding. However, the existence of these over-reactive ultra-large multimer can pose a risk for the occurrence of detrimental thrombotic side effects. A tight regulation of vWF multimer size distribution is essential. [6] Therefore, the ultra-large vWF multimer are digested to smaller fragments by a disintegrin and metalloprotease named ADAMTS13 and

undergoes scission to shorten the chain to its typical length, after being released by endothelial cells. [11–15] After cleavage, the vWF concatemers in plasma can contain up to 40 to 200 monomers that can be stretched by shear flow and extended to tens of microns. After synthesis and removal of the signal peptide, pro-vWF subunits associate in the endoplasmic reticulum in “tail-to-tail” dimers by the formation of disulfide bonds between CK domains. Following this, dimers further polymerize by forming “head-to-head” disulfide bonds between the amino-terminal cysteine-rich D3 domains before secretion (Fig. 1-1 (A)). With such enormous length, multimeric vWF carries many binding sites for platelets and collagen, and experiences highly significant hydrodynamic forces in the circulating system. It has been reported that vWF has force-sensing capability: the protein adopts a compact shape in normal circulatory status where shear rates range from hundreds to a few thousand per second; for shear rates greater than 5000 s^{-1}, vWF changes conformation to an elongated shape, increasing its interaction with platelets and collagen. (Fig. 1-1 (B))

At the tertiary structural level, each pro-vWF subunit consists of 4 types of repeated domains that are arranged in the sequence D1-D2-D’-D3-A1-A2-A3-D4-B1-B2-B3-C1-C2-CK (Fig. 1 (A)). Individual domains contain the various chemical functionalities required for the interactions between vWF and its surrendings. [8] Uniquely among domains in vWF, A2 domain is a force-sensitive domain that lacks a long-range disulfide and thus can be completely unfolded by elongational force, such as high shear flow or elongational flow. [8,15] Unfolding of A2 has an important functionality that dictates the cleavage of vWF multimers through with ADAMTS-13.

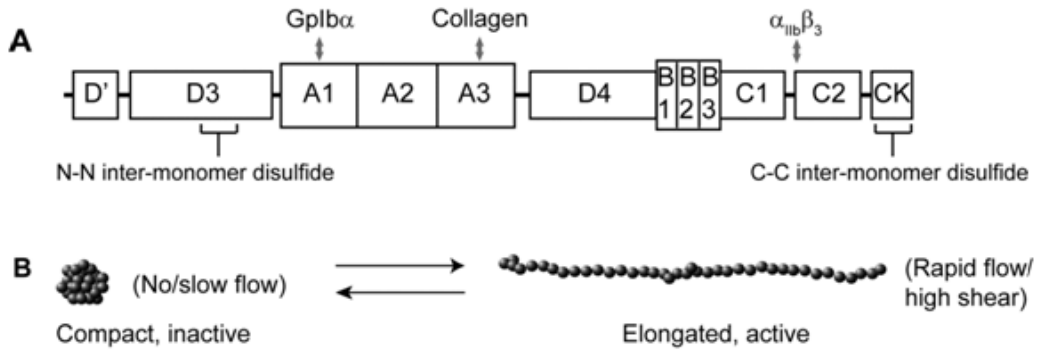

Fig. 1.3.1 (A) Schematic illustration of vWF's domains. (B) Possible mechanism of flow-induced conformational change.

This is a regulatory process that is known to occur throughout the bloodstream as a way to limit the length of vWF and prevent unnecessary thrombus formation. [10,15] A1 domain interacts strongly with platelets through glycoprotein (GP)1ba on the platelet surface. GP1ba receptor has a N-ternimal leucine-rich repeat (LRR) horseshoe-shaped domain followed by an anionic region with sulfated tyrosines, important in binding to thrombin. Remarkably, as A1 domain is the most positively charged domain in vWF and the face of GP1ba receptor is negatively charged, electrostatic interactions aid in coupling of this ligand-receptor pair. [8,10] The role of this interaction appears to be the capture and incorporation of platelets into plug, which initiate the blood-clotting cascade. Interestingly, A1 domain also has binding sites for fibrillar collagens, although mutagenesis studies suggest the major collagen binding site of multimeric vWF is within domain A3. A1 binds collagen VI, a microfibrillar collagen and binds collagens I and III less well. [8] Since the interaction of the A3 domain with fibrillar collagen is considered to be dominant, its structure has been determined to consist of a central hydrophobic parallel β–sheet surrounded by several α–helices in an open α/β sheet or dinucleotide-binding fold. [7] The C1 domain carries the ubiquitous Arginine-Glycine-Aspartic Acid

(RGD) sequence that is well known as the primary ligand that binds to integrins. [16] In a particular case, the C1 domain also serves to bind to the αIIbβ3 integrin that is expressed on the surface of platelets. [6] This interaction between C1 domain and platelets further promoted platelet aggregation, leading to additional recruitment of platelets from the blood stream. [6,8,10] These constitute most important parts in vWF monomers and the domain structures provide major binding sites interacting with a physiological environment under proper conditions. Interestingly, the interactions between vWF multimer and collagens or platelets are largely suppressed in a quiescent blood vessel. The fluid flow activation is required in order for vWF multimer to function in its desired capacity. For example, strong elongational flow or shear flow, which is normal close to damaged vessel wall, is able to elongate vWF multimer that will expose multiple binding sites in a physiological environment and facilitate blood clotting process eventually. This unique behavior of vWF multimer in human blood is definitely inspiring. Comprehensive studies will help to develop novel drug delivery method that use a molecule as the vehicle that carries specific drug molecule directly to the targeting sites in a precise and controlled fashion and therefore diminish the side effects typically seen when these drugs end up in healthy tissues. Manipulating the flow behavior at the targeting sites rather than changing the pH or temperature, we are able to induce a “stimulus-response” system at a desired location in the human body.

Chapter 2 von Willebrand Factor Simulation Methodology

2.1 von Willebrand Factor Model

Many studies have used coarse grain molecular models to understand macromolecule behavior, including specific mechanisms by which vWF senses flow. These models typically employ some form of bead-spring description of the biopolymer. In such models, a single bead may represent a monomer or part of a monomer and adjacent beads in a polymer are connected by finitely extensible non-linear elastic (FENE) springs. [17] Beads, including those not connected by springs, typically interact via a pair potential such as the Lennard-Jones. Instead of springs, one can utilize a pair potential description between bound beads where, perhaps, the bound interaction is much stronger than the un-bound bead-bead pair potential. Such an approach is useful if molecular scission is relevant to the phenomenon being modeled. This approach was described as the potential model (PM) in a recent review. [18] An alternate method for defining binding between beads was described as the reactive model (RM) and, in such descriptions; bonds between beads are formed stochastically based on proximity and parameterized binding and unbinding energies. This latter approach is particularly appealing for describing binding between vWF and relevant biological species, like platelets and tissue walls.

Alexander-Katz and his coworkers [19,20] used PM methods to investigate the unfolding phenomenon of polymers under the influence of both shear flow and elongational flow. They found unfolding is regulated very strongly by elongational flow fields, compared to shear flow. Schneider et al. [21] utilized the same kind of model in their simulations. They observed flow-induced conformation changes both in experiments and simulations,

and concluded there is a critical shear rate to unfold vWF in bulk, which triggers surface adsorption in the presence of a collagen substrate. A reactive model approach was used by Sing, *et al.* to investigate the force-extension behavior of self-associating homopolymers. [22] They utilized the same RM technique as implemented in the Bell model to describe the interaction between A3 domains on vWF multimers and collagen. Using this method, they were able to study vWF adsorbing and immobilizing platelets at sites of injury under high-shear-rate conditions. [23] Those results showed the expected shear-induced adsorption behavior and the adhesion rate quantitatively matched experimental observations. Other important simulation work was done by Ibanez-Garcia et al. [24] They studied the effect of attractive surfaces on the stretching of confined tethered polymers under shear flow and found that adsorption is enhanced by the shear flow strength in agreement with simulations of adsorbed non-tethered polymers. Results described here provide a sampling of work already present in the literature and it is obvious that distinct benefit can be had from applying different modeling techniques, especially coarse-graining on disparate length scale.

2.1.1 Mapping vWF from Biological Structure to Physical Model

von Willebrand Factor has extremely complicated structure as described in the introduction section of this dissertation, largely due to its various domains performing numerous functions. However, a good physical property of vWF multimers is that the monomers are linked head-to-head and tail-to-tail into ultra long concatemers, which vastly simplify the model process. The overall molecule, in an unraveled state where repeat units can be envisioned to roughly line up, can span tens of microns. This scale is

associated with molecular function in the sense that vWF proteins must have at least ten repeat units to express functionality. At a smaller length scale of order tens to one hundred nanometers are the individual repeat units; these monomers consist of a collection of folded domains, each with a specific chemical binding affinity. Collectively, these domains help unraveled vWF molecules execute necessary binding to platelets and tissue walls (as well as many other complex biochemical reactions). Thus, when considering the mechanical response of vWF, two scales of unfolding must be addressed: on the larger length scale is unfolding of the overall molecule as monomers become more lined up; on the smaller length scale is unfolding of individual domains, which may be critical to proper chemical activity of the polymer.

Prior experimental work has been advanced investigating vWF-unfolding behavior on both length scales described above. Direct visual tracking has been achieved of unfolded vWF polymers and their dynamics on a full molecule scale. [21] In addressing the mechanical response of sub-monomer units, a significant breakthrough was made by Zhang, *et al.*, which is central to the model introduced here. Using single molecule force spectroscopy methods, they showed the inner structure and mechanical characteristics of a vWF monomer's domains. [15] Their work pointed out that the A2 domain of vWF, which lacks protection by disulfide bonds, could be unfolded with applied forces that, though non-trivial, may indeed manifest under very rapid blood flow conditions. Furthermore, relative to the size of an unextended monomer, the A2 domain demonstrates a large degree of elongation via unfolding. Specifically, A2 domain force-extension data in Ref. [15] showed distinct unfolding events and that, for an applied force near 20 pN, an overall extension near 50 nm occurred. Exerting hydrodynamic forces in the range of

10-20 pN on molecules, even those as large as vWF, is non-trivial; nonetheless, in rapid blood flow conditions, it is estimated that such forces do indeed reach of order 10 pN, driving A2 domain unfolding. [15] The overall processes in which vWF engages during blood clotting are much more complex than simply unfolding; however, experimental data suggest that unfolding of the A2 domain is an important process in determining vWF behavior as it responds to rapid blood flow.

Here, a new vWF model is presented that attempts to more realistically describe molecular architecture inherent in the protein. Specifically, the model captures aspects of what we believe to be a primary mechanical response of a single monomer, as well as adjacent monomer-monomer mechanics. This is accomplished by modeling vWF monomers as an extensible domain with relatively rigid domains on either side of it. The A2 domain has been shown to undergo significant unfolding during single molecule stretching experiments. [15] The extensible regions, or domains, on a vWF monomer are thus modeled as a FENE spring capable of significant extension. At each end of the spring is a spherical bead to represent neighboring rigid domains (Fig. 2-1 (b)). Adjacent monomers are connected by a relatively stiff harmonic spring between a bead on each monomer, thus forming vWF multimers of desired length. This straightforward modification of typical coarse-grain vWF models produces a still relatively simple model that is capable of capturing some of the structural complexity of vWF multimers. [25]

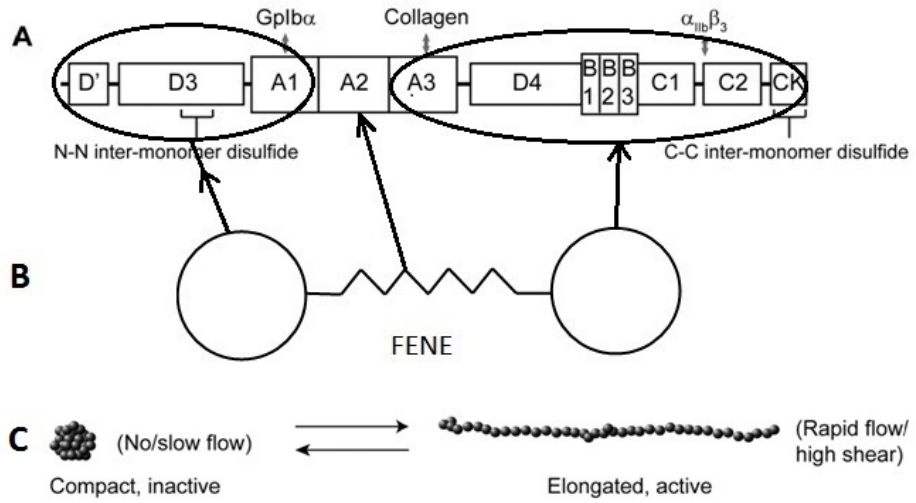

Fig. 2.1.1 (A) Schematic illustration of vWF's domains. (B) The vWF monomer model containing two rigid beads connected by a highly flexible FENE spring. (C) Possible mechanism of flow-induced conformational change.

2.1.2 Associating Surfaces Model

After we successfully elucidate the biological structure of vWF multimer in the physical modeling perspective, the study has to be broaden to include more interactions in the context of vWF multimer's functionality in blood clotting, like the interactions between vWF multimer and platelets or the collagens. [6,8,10] Specifically, the GP1ba receptor that binds between the vWF A1 domain and platelet surface is known to display novel flexible bond type behavior, where a high-affinity state is activated by force to reveal longer-lived slip bond behaviors. [26] Apparently the Lennard-Jones model is not sufficient to describe the physics underlying the behavior exhibited by vWF both in *vitro* and in *vivo*, because the hydrodynamic interactions between surface and the chains will cause so-called hydrodynamic life in the surface limit, which leads to the desorption of polymers from the attractive surface ultimately. [27–36] In order to resolve these

apparent contradictions between vWF and fundamental polymer theory, we introduce the Bell model interactions as a way to more accurately represent the interaction between the polymer and the surface. [37–39] Basically, this novel interaction is to mimic the binding behavior between the vWF A3 domain and extracellular matrix collagens, which is a ubiquitous way to parameterize a complicated energy landscape in a facile manner by defining interacting entities as either bound or unbound. The rate of transition between the two states is governed by the height of an intermediate energy barrier between them, with a large barrier impeding both the forward and backward transitions and a small barrier allowing rapid binding and unbinding. The activation energies of binding and unbinding, which control the probabilities of binding and unbinding between A3 domain of vWF multimer and collagen, were measured experimentally by force spectroscopy and were extracted using the Dudko-Hummer-Szabo model under different temperatures. [26,39]

2.2 Numerical Method

The vWF model here is modified from the bead-spring model that has been used by many authors. [40,41] In the present model, each monomer forming the vWF multimer consists of one FENE spring that connects two beads. The rationale is that experimental evidence exists indicating the A2 domain of each monomer can experience unfolding due to forces exerted on vWF molecules at the highest rates of blood flow in the human body. From a mechanical response point of view, it is more realistic to represent the extensible part of each monomer as a FENE spring than to represent the whole monomer as a single bead. Furthermore, the use of a highly (but finitely) extensible spring is more computationally

efficient than modeling the A2 domain as a relatively long series of beads. To form vWF multimers, adjacent monomers in our model are connected by a relatively stiff harmonic spring, representing the inter-monomer disulfide bonds. A Lennard-Jones pairwise interaction is applied between beads.

2.2.1 Brownian dynamics

The Brownian Dynamics is a simplified version of Langevin dynamics, in which the average acceleration can be neglected. So BD is also named non- inertial dynamics. Briefly, Langevin dynamics uses a stochastic differential equation in which two force terms have been added to Newton's second law. Since a molecule in the real world is not present in a vacuum and solvent molecules causes friction and collisions to perturb the system. The BD simulation, an extremely efficient method for treating molecular, is proposed as early as 1978 by D.L. Ermak and J.A. McCammon. [42] They present BD simulations of short chains with hydrodynamic interaction (HI) at equilibrium. Almost at the same time, Fixman developed and applied the mathematical background for performing BD simulations of polymer chains in flow. [43] BD simulations of FENE dumbbell models with HI and excluded volume (EV) effects were simulated by Rudisill and Cummings. [44] More recently, J.S. Hur and R.G. Larson simulated single DNA molecules in shear flow using BD simulations and the simulation results, especially in light of the excellent agreement with experiment, demonstrated the basic physical elements necessary for any rheological model to capture the dynamics of single polymer chains in flow. [45] Later M. Chopra and R.G. Larson extended the BD simulations into isolated polymer molecules in shear flow near adsorbing and nonadsorbing surfaces. [46]

2.2.2 Physical forces

The drag force is the friction force that flowing solvent exerts on the polymer and is given by,

$$\boldsymbol{F}_i^D = -\zeta(\dot{\mathbf{r}}_i - \boldsymbol{v}_i) = -\zeta(\dot{\mathbf{r}}_i - (\nabla \boldsymbol{u})^T \mathbf{r}_i) \quad (1)$$

where ζ is the drag coefficient, $\dot{\mathbf{r}}_i$ is the velocity of the bead i , $\boldsymbol{v}_i$ is the undisturbed velocity field and $\nabla \boldsymbol{u}$ is the velocity gradient tensor. Similar to Hoda and Larson's work [16], variables are made dimensionless by scaling length with $\sqrt{k_b T/H}$, force with $\sqrt{H k_b T}$, and time with ζ/H, where k_b is Boltzmann constant, T is the absolute temperature and H is the spring constant in the FENE spring term. $\boldsymbol{F^S}$ is either a FENE spring force or a harmonic spring force, which account for the connectivity of the chain. Dimensionless FENE springs are described as

$$\boldsymbol{F}_{FENE}^S = \frac{\boldsymbol{Q}_i}{1 - {Q_i}^2/Q_0^2} \quad (2)$$

where $\boldsymbol{Q}_i = \mathbf{r}_{i+1} - \mathbf{r}_i$ and Q_i is the magnitude of $\boldsymbol{Q}_i$. Q_0 is the maximum extended length for the FENE spring. The expression for the harmonic springs is given by

$$\boldsymbol{F}_{Harmonic}^S = k\frac{\boldsymbol{Q}_i}{Q_i}(Q_i - \dot{Q}) \quad (3)$$

The harmonic force of strength k keeps the average distance between connected monomers stiffly constrained to relatively small fluctuations around $\dot{Q}$. To ensure this, the value of k is chosen to be 100. $\dot{Q}$ = 4 (21.54 nm) which is slightly larger than two times the bead radius, determined from size considerations for vWF monomers. The self-association between different monomers, which collapses the vWF multimer into a

relatively compact globule, is represented by a pairwise truncated Lennard-Jones interaction force that acts between beads.

$$\mathbf{F}_{ij}^{In} = \frac{4}{d^{ev}}\begin{cases}\left[12\left(\frac{d^{ev}}{r_{ij}}\right)^{13} - 6\varepsilon\left(\frac{d^{ev}}{r_{ij}}\right)^{7}\right]\hat{\mathbf{r}}_{ij} & r_{ij} \geq 3 \\ \left[12\left(\frac{d^{ev}}{3}\right)^{13} - 6\varepsilon\left(\frac{d^{ev}}{3}\right)^{7}\right]\hat{\mathbf{r}}_{ij} & r_{ij} < 3\end{cases} \quad (4)$$

where $\mathbf{r}_{ij} = \mathbf{r}_i - \mathbf{r}_j$, $r_{ij} = |\mathbf{r}_{ij}|$, $\hat{\mathbf{r}}_{ij}$ is the unit vector along $\mathbf{r}_{ij}$, and ε and d^{ev} are the energy and length parameters, respectively, whose values are addressed below. The Brownian force is $\boldsymbol{F}^{B} = (\frac{6k_BT\zeta}{\Delta t})^{1/2}\boldsymbol{n}$, where $\boldsymbol{n}$ is a random three-dimensional vector, each component of which is uniformly distributed in the interval $[1, -1]$. The reason we truncated the Lennard-Jones Potential is to make sure the stability of the simulations even when two beads are overlapping with each other. The truncated distance is chosen to produce the same level of maximum repulsive force as Larson's paper. [40]

To prevent vWF multimer crossing the planar surface, a nine-three Lennard-Jones potential is used

$$\boldsymbol{F}^{Wall} = \frac{3\sqrt{3}}{2d_{wall}^{ev}}\left[9(\frac{d_{wall}^{ev}}{z_i})^{10} - 3\varepsilon_{wall}(\frac{d_{wall}^{ev}}{z_i})^{4}\right]\hat{\mathbf{z}} \quad (5)$$

$\hat{\mathbf{z}}$ is the unit vector in the direction normal to the wall, z_i is the distance between the center-of-mass of the bead and the wall, ε_{wall} and and d_{wall}^{ev} are energy and length parameters of the bead-wall interaction, respectively. The bond formed between A3 domain of vWF multimer and collagen is simulated by $\boldsymbol{F}^{Bond}$. The bond force is expressed as a harmonic spring

$$\boldsymbol{F}^{Bond} = k\frac{\boldsymbol{q}_i}{q_i}(q_i - \dot{q})w_{i,j,t} \quad (6)$$

$\boldsymbol{q}_i$ is the location of bead i minus the location of the binding site ,q_i is the magnitude of $\boldsymbol{q}_i$ and $\dot{q}$ is the equilibrium length of the bond. $w_{i,j,t}$ is an time-evolution matrix accounting the status of the binding between monomer i and a surface binder j at time t, with 1 indicating that there is a binding and 0 indicating the absence of a binding interaction. The evolution of the matrix, $w_{i,j,t}$, is governed by

$$w_{i,j,t} = \begin{cases} \begin{cases} 1 \ if \ \Xi < e^{-\Delta E_B} \\ 0 \ if \ \Xi > e^{-\Delta E_B} \end{cases} & if \ w_{i,j,t-1} = 0 \ and \ q_i \leq \tilde{q} \\ \begin{cases} 0 \ if \ \Xi < e^{-\Delta E_{UB} + \dot{f}\dot{r}} \\ 1 \ if \ \Xi > e^{-\Delta E_{UB} + \dot{f}\dot{r}} \end{cases} & if \ w_{i,j,t-1} = 1 \end{cases} \tag{7}$$

The state of $w_{i,j,t}$ depends on the binding transition probabilities $e^{-\Delta E_B}$ and $e^{-\Delta E_{UB}}$, the previous state $w_{i,j,t-1}$, and reaction radius $\tilde{q}$ within which the reaction may occur. ΔE_B and ΔE_{UB} represent the activation energies of binding and unbinding, respectively. Ξ is the randomly generated number between 0 and 1. $\dot{f}$ is the external force along the polymer-binder interactions and $\dot{r}$ is the spatial distance from the minimum of the bound potential well to the energy barrier along the reaction coordinate. The corrected RPY tensor with a correction term that accounts for the no-slip condition at the wall can be found at Ref [30,31].

2.2.3 Governing equations

The governing equations in the inertia free limit are obtained by a force balance on each bead:

$$\boldsymbol{F}_i^D + \boldsymbol{F}_i^S + \boldsymbol{F}_i^{In} + \boldsymbol{F}_i^B = 0, i = 1,2, \dots, N \tag{8}$$

where the subscript i refers to the bead number and $\boldsymbol{F}_i^D$, $\boldsymbol{F}_i^S$, $\boldsymbol{F}_i^{In}$ and $\boldsymbol{F}_i^B$ are the hydrodynamic (viscous) drag force, the spring force (either FENE or harmonic), the bead-bead interaction force, and the Brownian force, respectively.

In the absence of hydrodynamic interaction (HI), we are in the free draining (FD) limit. To explore the importance of HI in determining dynamics for our new model, the Rotne-Prager-Yamakawa (RPY) tensor was utilized. The disturbed velocity $\boldsymbol{v}_i'$, produced by another bead j, is a linear function of the hydrodynamic drag force $\boldsymbol{F}_j^D$,

$$\boldsymbol{v}_i^{'} = -\boldsymbol{\Omega}_{ij}\boldsymbol{F}_j^D = \boldsymbol{\Omega}_{ij}\left(\boldsymbol{F}_j^S + \boldsymbol{F}_j^{BB} + \boldsymbol{F}_j^B\right) \tag{9}$$

where $\boldsymbol{\Omega}_{ij}$ is the hydrodynamic interaction tensor between two beads. Ermak and McCammon [42] showed that the disturbance velocity can be included into the Langevin equation by introducing the diffusion tensor $\mathbf{D}_{ij} = \frac{k_B T}{\zeta}\left(\delta_{ij}\mathbf{I} + \zeta\boldsymbol{\Omega}_{ij}\right)$, where δ_{ij} is the Kronecker delta.

The RPY tensor is given by [20,43,47]

$$\boldsymbol{D}_{ii} = \boldsymbol{I} \tag{10}$$

$$\boldsymbol{D}_{ij} = \frac{3}{4}\frac{a}{r_{ij}}\begin{cases}\left[\left(1+\frac{2a^2}{3r_{ij}^2}\right)\boldsymbol{I}+\left(1-\frac{2a^2}{r_{ij}^2}\right)\frac{\mathbf{r}_{ij}\mathbf{r}_{ij}}{r_{ij}^2}\right], & r_{ij}\geq 2a \\ \frac{r_{ij}}{2a}\left[\left(\frac{8}{3}-\frac{3r_{ij}}{4a^2}\right)\boldsymbol{I}+\frac{r_{ij}\mathbf{r}_{ij}\mathbf{r}_{ij}}{4a\ r_{ij}^2}\right], & r_{ij}<2a\end{cases} \tag{11}$$

A square root relationship exists between $\boldsymbol{D}_{ij}$ and $\boldsymbol{\sigma}_{ij}$, [47]

$$\boldsymbol{D}_j = \sum_{l=1}\boldsymbol{\sigma}_{il}\cdot\boldsymbol{\sigma}_{lj} \tag{12}$$

After substituting and rearranging, the stochastic differential equation including HI becomes,

$$\dot{\mathbf{r}}_i = (\nabla \mathbf{u})^T \mathbf{r}_i + \sum_{j=1}^{N} \frac{\mathbf{D}_{ij} \cdot \left(\boldsymbol{F}_j^S + \boldsymbol{F}_j^{BB}\right)}{k_B T} + \left(\frac{6}{\Delta t}\right)^{1/2} \sum_{j=1}^{i} \boldsymbol{\sigma}_{ij}\, \boldsymbol{n}_j \tag{13}$$

By applying dimensionless units, the governing equation is,

$$\mathbf{r}_i = \mathbf{r}_i^{old} + \left[(\nabla \boldsymbol{u})^T \cdot \mathbf{r}_i + \sum_{j=1}^{N} \boldsymbol{D}_{ij} \left(\boldsymbol{F}_j^S + \boldsymbol{F}_j^{BB}\right)\right]\Delta t + \sqrt{6\Delta t} \sum_{j=1}^{i} \boldsymbol{\sigma}_{ij}\, \boldsymbol{n}_j \tag{14}$$

where $\mathbf{r}_i$ and $\mathbf{r}_i^{old}$ are the position vectors of bead i at the new and old times respectively. Incorporating the interactions between surface and vWF multimer into the governing equations, it becomes,

$$\mathbf{r}_i = \mathbf{r}_i^{old} + \left[(\nabla \boldsymbol{u})^T \cdot \mathbf{r}_i + \sum_{j=1}^{N} \boldsymbol{D}_{ij} \left(\boldsymbol{F}_j^S - \boldsymbol{F}_{j-1}^S + \boldsymbol{F}_j^{BB} + \boldsymbol{F}_j^{Wall} + \boldsymbol{F}_j^{Bond}\right) + \sum_{j=1}^{N} \boldsymbol{\nabla_j} \cdot \boldsymbol{D}_{ij}\right]\Delta t + \sqrt{6\Delta t} \sum_{j=1}^{i} \boldsymbol{\sigma}_{ij}\, \boldsymbol{n}_j \tag{15}$$

The hydrodynamic interactions are taken into account via the diffusivity tensor $\boldsymbol{D}_{ij}$ whose explicit expression will be given in Appendix A. The term $\boldsymbol{\nabla_j} \cdot \boldsymbol{D}_{ij}$ compensates for the spurious flux due to inhomogeneities in the self-mobility. The tensor $\boldsymbol{\sigma}_{ij}$ is obtained from a Cholesky decomposition of $\boldsymbol{D}_{ij}$.

2.3 Parameterization of vWF and associating surface model

Parameters used in the vWF model described above were obtained by optimizing against experimental data, where available. For parameters in the FENE spring, data from Ref.

[15] were used to compute H = 0.1428 mN/m and $Q_0 = 60\ nm$. These two values were obtained by performing a curve-fit to the A2 domain force-extension data using the FENE spring law. [15] Note that the A2 domain exhibits detectable extension only when the force exceeds a certain threshold value. The present model doesn't consider such a finite force onset of elongation. Possible impacts this may have on data presented are discussed below; a finite force onset model is under development and its effect on the dynamics of vWF will be investigated in a future study. In the simulations, the remaining parameters to be decided were the bead radius a, as well as the energy parameter ε and the length parameter d^{ev} for the Lennard-Jones potential. The radius of bead a = 10 nm, which is half of the length of the fully unfolded monomer (80 nm) minus the maximum extended length for the FENE spring Q_0. The length parameter in the Lennard-Jones potential $d^{ev} = 2a/2^{1/6}$. To model the vWF multimer as being in a poor solvent, it should be in a globule state at zero and low flow regimes. This was achieved with an energy parameter ε = 1.43 without units. Temperature is fixed at T = 300 K for all simulations. The length and force are made dimensionless by scaling with $\sqrt{k_bT/H} = 5.3846\ nm$ and $\sqrt{Hk_bT} = 0.7692\ pN$, respectively. Because the dynamic viscosity μ of phosphate buffered saline solvent is almost the same as water, which is 1 Ns/m^2, the drag coefficient is $\zeta = 6\pi\mu a$ =1.8848 × 10^{-10} $N \cdot s/m$ and the time scale is $\zeta/H = 1.319\ \mu s$.

Parameters used in associating surface model includes the activation energies of binding and unbinding of the bell model, 2.9 K_BT and 22.9 K_BT correspondingly, which were measured experimentally by force spectroscopy and were extracted using the Dudko-Hummer-Szabo model under different temperatures. Such experimental measurements

are conducted by the present authors and will be published in another paper. Usually the density of the collagen used in experiments is roughly around 8 mg/ml and the molecular weight of the collagen is $4 \times 10^5\ g/mol$. Simple calculation shows the distance between each collagen on the surface will be 8.1 without units if they are homogenously dispersed.

2.4 Simulation details

2.4.1 Criterion for diluteness of solvent

The "diluteness" has a very important meaning in polymer science, which the polymer concentration is low enough that the polymers do not interact with each other topologically or hydrodynamically. [48] Thus, we can assume the effect of polymers on rheological properties of the fluid is linear. Experimentally and theoretically, there exist three concentration regimes: dilute, semi-dilute, and concentrated. And it is hard to establish a well-defined transition concentration separating regimes with distinctive features, i.e. to find a measurable quantity displaying a different behavior depending on the actual regime. [49] A simple criterion for diluteness of a polymer solution is given by [48]

$$c < \frac{1}{[\eta]_0} \tag{16}$$

where $[\eta]_0$ is the intrinsic viscosity of the polymer in dilute solution and is defined as

$$[\eta]_0 = \lim_{c\to\infty} \frac{\eta-\eta_s}{c\eta_s} \tag{17}$$

where η is the solution viscosity and η_s is the viscosity of the solvent. The subscript "0" in $[\eta]_0$ means that it is measured at low shear rates, where it reaches an asymptotic plateau value that is independent of shear rate. The critical "diluteness" condition has a huge impact on the complexity of simulations. Once we make sure the solvent is dilute, the Brownian dynamics simulation can be simplified to exclude the interactions between different polymer chains, e.g. entanglements and only one vWF multimer need to be initialized and taken into consideration during one simulation run. Experimental results show that the propeptide vWF (vWFpp) has a concentration in plasma of 1 µg/ml and a T½ of 2-3 hours whereas the mature VWF protein has a concentration in plasma of 10 µg/ml and a T½ of 8-12 hours. [50] It confirms our hypothesis that vWF multimers are dilute solved in the human blood and the dynamics of vWF multimers in human blood are studied by considering a single chain conformational change in different flow conditions and complex geometries.

2.4.2 vWF multimer initialization

Generally, there are two different methods used to get the initial conformation of a single vWF multimer. The first method generates the initial conformation by placing the first bead at origin, and subsequent beads at random directions and at certain fixed distance away from the beads that precede them. Whereas the other one takes the same procedures as mentioned in the first method as the first stage. The second stage of the second method is to take the conformation got in the first stage and run the MD simulation in the equilibrium state until it reaches plateau. The conformation at the end of the second stage is taken as the initial conformation of a vWF multimer, which is used later in different flow conditions and complex geometries.

Here, The initial conformation was generated by placing the first bead at the origin; subsequent beads were placed either 4 or 5 dimensionless units away from the preceding bead, depending on whether the two beads were connected by a harmonic or FENE spring, respectively. The actual position of placement was chosen randomly but to avoid unphysical overlaps with previously placed beads. The reason the second stage is neglected in our simulation is that it has little influence on the final results. Importantly, 32 different initial conformations were initialized in different runs in order to improve statistics. Simulations were conducted to characterize the motion of vWF multimers for 100 times longer than their computed longest relaxation time.

2.4.3 Choosing time-steps

The selection of time-step Δt was dependent on whether the model was run with or without hydrodynamic effect. For free draining (FD) case, the simulations were conducted using the time-step of $\Delta t = 10^{-4}$. Whereas the time-step Δt chosen for HI cases can be divided into two categories: one is to update the position of each bead, i.e. update the governing equation and the HI matrix at the same frequency; the other is using different time-steps Δt for the governing equation and the HI matrix. All simulations of HI cases used the time-step $\Delta t = 10^{-5}$ for the governing equation, no matter which category it is. Compared the simulation results between these two categories, we found they are almost the same if the time-step Δt for the HI matrix is updated ten times less frequently than the governing equation.

2.4.4 Quantity of interests

The radius-of-gyration was used to characterize the conformation of a vWF multimer and is defined as,

$$R_g = \sqrt{\frac{\langle \sum_{i=1}^{N} |\mathbf{r}_i - \mathbf{r}_{c,m}|^2 \rangle}{N}} \tag{18}$$

where $\mathbf{r}_i$ is the position of ith bead, $\mathbf{r}_{c,m}$is the center of mass of the chain and $\langle \cdot \rangle$ denotes an ensemble average. The R_z is used to characterize the relative position between the polymer and chain and the wall. And it's written in the form:

$$R_z = \frac{\langle \sum_{i=1}^{N} |z_i - z_w| \rangle}{N} \tag{19}$$

where z_i is the position of the bead at z direction, and z_w is the position of the wall. The adhesion rate is characterized by the percentage of polymer chains that have binding interactions with the collagen-coated wall. The length of FENE springs is of great interests in this thesis because of its important physical and biological meaning, representing the A2 domain and is quantified by averaging over all FENE springs in all vWF chains after the simulation reaches equilibriums.

2.4.5 Flow condition

The vWF multimers were modeled in quiescent solvent or in fluid flow. Only two flow conditions are investigated in this thesis: shear flow and poiseuille flow. For a pure shear flow, the velocity gradient of the flow field was given by

$$\nabla \mathbf{u} = \begin{pmatrix} 0 & 0 & \dot{\gamma} \\ 0 & 0 & 0 \\ 0 & 0 & 0 \end{pmatrix} \tag{20}$$

and $\dot{\gamma}$ is the shear rate. For poiseuille flow, the shear rate $\dot{\gamma}$ is a linear function of the position of beads relative to the boundary.

Chapter 3 Flow-induced conformation changes of homopolymers

3.1 Introduction

In order to understand vWF's behavior in vivo, we started with a straightforward in *vitro* setup by considering a collapsed homopolymers in an infinite medium under the influence of fluid flow. The bio-molecule is collapsed in a quiescent vessel and activates in the presence of a fluid flow. This conformational transition from coiled states to stretched states is a widely studied area of polymer science for several decades. Pioneering works has been done by De Gennes in 1974, which conclude a solute polymer coil should unwind abruptly when a certain critical value of the velocity gradient is reached. [51] The research has been active on and off, until Axel Buguin et al. investigate the grafted polymer chains under strong flows. [52] This study gained a lot of interests in the beginning of twenty first century. E. Shaqfeh presented a study of the rheology and optical properties during the start-up of the uniaxial extensional and shear flow for freely draining using bead-rod model and applied this methodology into an examination of the dynamics of single-molecule DNA in the shear and extensional flow. [45,53–55] Meanwhile, D. Smith has observed the movement of individual, flexible polymers in both steady shear and elongational flow by the use of video fluorescence microscopy and simulated single DNA molecule under these flow conditions, which quantitative agreement has been obtained in various unraveling states. [54,56–58] The simulation techniques used in the studies mentioned above are free draining cases (FD), which neglect hydrodynamic interactions (HI). The effect of HI has been included in Brownian dynamics simulations by D. Petera [59] ; R. Jendrejack [47]; and C. Hsieh [41], which show significant influences on dynamics of polymer chains. Subsequently, R. Larson

concluded the progress toward understanding the rheology of dilute solution of flexible polymers and further developed the simulation methodology by considering self-entanglements. [40,48] A. Katz also innovated the Brownian dynamics simulations by include more realistic effects, i.e. HI and self-associating effects between adjacent molecules. [20,60] These research results constitute a broad context, regarding conformational changes of homopolymers in response to various flow conditions with or without various effects.

3.2 Flow-induced conformational change of vWF multimer

The progress in experiments testing the characteristic of vWF in fluid flow has been made by Ref [21,61,62], by placing fluorescently-labeled polymers into a sheared fluid and monitoring their elongation as a function of shear rate. Some analogous simulations using the novel vWF model described in Chapter II were conducted below to justify and verify the experimental results. The starting point for this situation for the work in this dissertation is the considering of vWF multimer in an infinite medium under the influence of fluid flow. The surfaces, which will be investigated exclusively in Chapter IV, are neglected here.

3.2.1 Calculation of the longest relaxation time

The Weissenberg number *Wi* is defined as the ratio of a viscoelastic fluid's relaxation time τ to some characteristic temporal scale. In simple shear flow, $Wi = \tau\dot{\gamma}$, where $\dot{\gamma}$ is shear rate. The longest relaxation time τ of vWF multimers varies with the number of repeat units, which here means the number of monomers. Because N is used to represent number of beads, the number of monomers is $N/2$. In order to compare simulation results

for vWF multimers with different length, the longest relaxation time τ was determined. We compute τ by starting with a model of an extended vWF chain whose end-to-end distance is 70% of its contour length *L*. A collection of such chains was modeled in no-flow conditions until the vWF chains were fully relaxed to their equilibrium end-to-end distance values. The relaxation time was then computed by fitting the square of the end-to-end distance $\langle R^2 \rangle$ versus time t in the regime where statistical errors are relatively small. [40]

$$\langle R^2 \rangle - \langle R^2 \rangle_{eq} = A\, exp(-t/\tau) \tag{21}$$

where $\langle R^2 \rangle_{eq}$ is the equilibrium value of $\langle R^2 \rangle$ and A is a constant. [41]

The relaxation curves for square of end-to-end distance versus time for *N* = 60 vWF multimers are shown in Fig. 2. The longest relaxation time τ was measured in the regime where the ratio of end-to-end distance to *L* is less than 0.3. [41,63] The *N* = 60 vWF multimer with HI is relaxing to a globule state faster than without HI. Simulations with three different initial conformations were done for the same number of beads; results from the simulations were essentially identical, indicating the initial conformation of vWF multimer has little influence on τ.

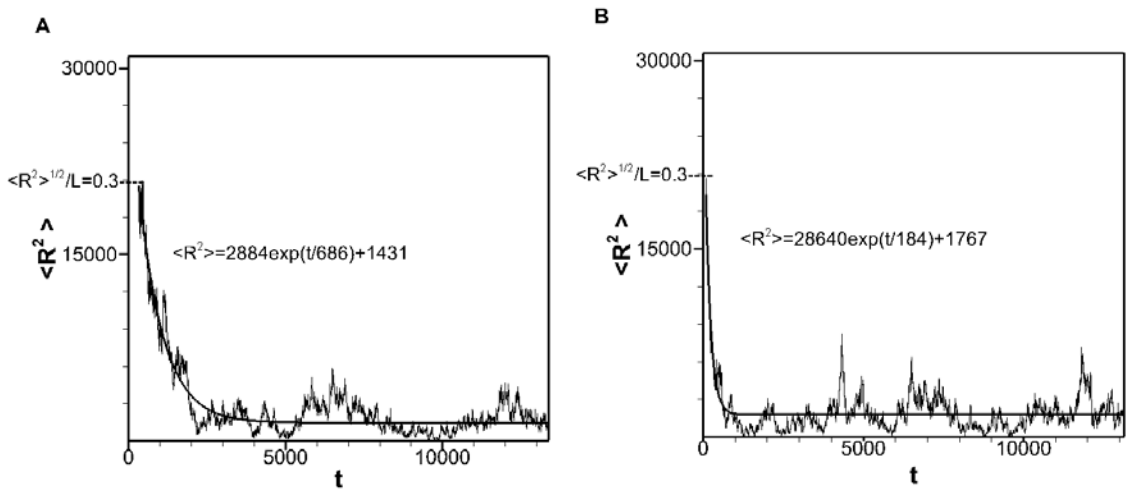

Fig. 3.2.1 Relaxation curves for square of end to end distance versus time using 60 beads (A) without HI and (B) with HI.

Figure 3 shows the longest relaxation time τ for different number of beads with and without HI. Data in Fig. 3 are averaged over 32 vWF multimers for each case, with different random number starting seeds and configurations. Results further emphasize that HI increases the rate of relaxation of vWF multimers to equilibrium from an extended state. Decreased relaxation time in the presence of HI is attributed to the so-called drag effect in that a preceding moving bead creates a stream pattern that pulls following beads in the direction of its motion. [64] It is found that a power-law scaling of relaxation time with number of beads exists, with exponents of 1.97 and 1.44 in simulations without and with HI. The R^2 values showing the quality of the fits are 0.9929 for FD and 0.9981 for HI. The exponents determined here agree well with the Rouse relaxation time (without HI) $\tau_R \sim N^2$ and the Zimm relaxation time (with HI) $\tau_Z \sim N^{3/2}$, which are predicted by polymer theory. [65]

The relaxation of vWF multimers was captured by S.W. Schneider et al. in experiments. [21] The fluorescence images of a video sequence acquired at 25 frames per second

showed that a 20 μm elongated vWF multimer relaxed back to its compact state in more than 160 ms and less than 320 ms. A very coarse estimate of the relaxation time based on the method used herein would thus be of order 100 *ms*. The length of an elongated vWF monomer is of order 80 *nm* to 100 nm; in the experiments of Ref. [21], vWF multimers were significantly, but not fully, elongated. Given this, a straightforward size consideration indicates that the vWF chain they studied had between 200 and 300 monomers. Considering this molecular size and using the power-law we get in our FD simulations, our prediction for relaxation time differs from experimental observation by at most a factor of two. Due to the simplistic nature of our model, our prediction is encouraging. However, an equivalent attempt to make such a comparison from data obtained with HI effect produces more than an order of magnitude discrepancy from experiment. We take this as indication that relaxation time as defined here is more appropriately predicted in a FD condition.

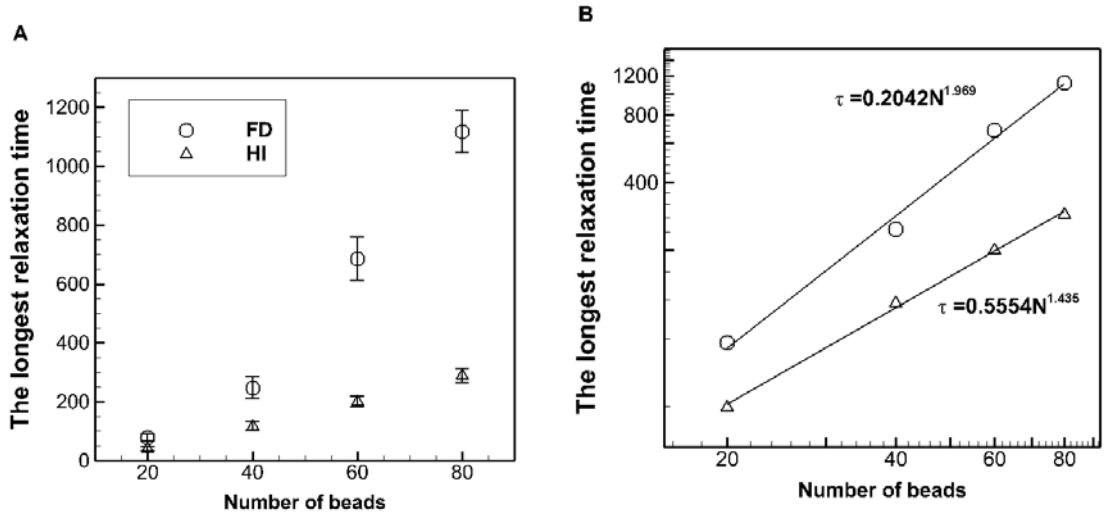

Fig. 3.2.2 Dependence of the longest relaxation time $\boldsymbol{\tau}$ on the number of beads $\boldsymbol{N}$ with and without hydrodynamics: (A) linear scale plot with error bar (confidence interval) and (B) log scale plot.

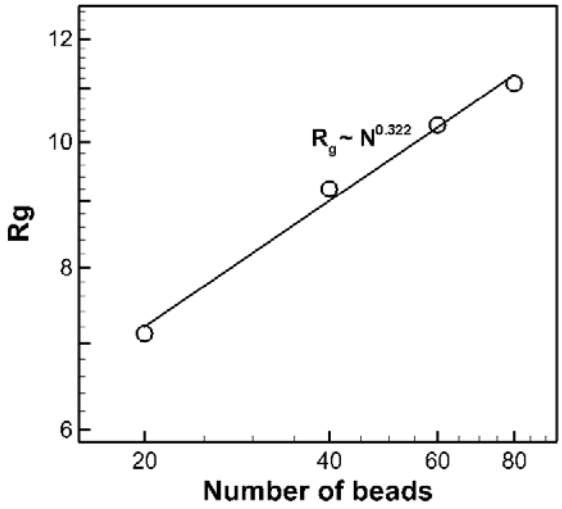

Fig. 3.2.3 Dependence of the radius-of-gyration $\boldsymbol{R_g}$ on chain length $\boldsymbol{N}$.

3.2.2 Calculation of molecular response in flow

Fig. 4 shows the dependence of radius-of-gyration on the length of vWF multimer in a no-flow condition (FD simulations). We found that R_g scales as $N^{0.322}$; that result is close to the predicted power law for polymers in poor solvent. Fig. 5 displays results during flow for the ensemble average of R_g normalized by $N^{0.322}$ as a function of Wi. As expected, normalized R_g monotonically increases with Wi and then approaches an apparent asymptote, regardless of the length of the vWF multimer, which is the same behavior that Larson observed. [40,54] Normalized R_g are approximately the same for all cases when Wi is below unity; in this limit of low flow, data for all cases shows little dependence on *Wi* and it is only for *Wi* > 1 that increasing R_g is observed. In addition, a gap between normalized R_g for different cases emerges and becomes more pronounced as Wi goes above unity. This is because longer vWF multimers have a greater number of dynamic structural modes through which they interact with imposed flow fields. Thus,

longer molecules have more potential to unfold and are more sensitive to high rate flow conditions.

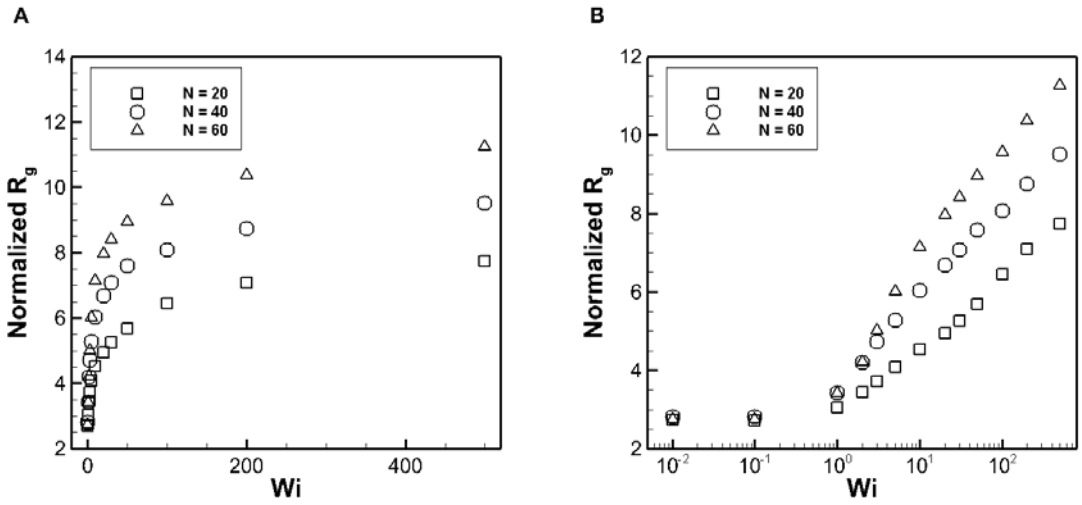

Fig. 3.2.4 Dependence of the normalized radius-of-gyration $\boldsymbol{R_g}$ for different length of chains on Weissenberg number ($\boldsymbol{Wi}$): (A) linear scale plot and (B) log scale plot.

Temporal characteristics for a single $N = 60$ vWF multimer under no flow condition and in $Wi = 1$ and 10 shear flow are represented in Fig. 6. As we see from the $Wi = 10$ case, the vWF multimer reacted rapidly to the shear flow such that there is no apparent transient state. In that case, the ensemble average of R_g was calculated by averaging all data during a simulation run. For this specific 60-bead vWF multimer, the simulation yielded an ensemble average $R_g = 21.42$ and standard deviation $\sigma = 8.99$. As we can see, the vWF multimer is significantly uncoiled at some points, which can enable the A3 domain to bind to collagen. A very coarse estimate of the fluctuation period for the $Wi = 10$ case is somewhat less than 1000 reduced units; the longest relaxation time computed for this N was 700, in agreement with fluctuation dynamics. Compared to the $Wi = 10$ case, the vWF multimer exhibits fewer unfolding events and overall smaller fluctuations in the $Wi = 1$ case, in which the assemble average $R_g = 11.058$ and standard deviation

$\sigma = 3.53$. However, occasional significant unfolding of vWF multimers still occurs at this relatively weak flow. This emphasizes the sensitivity of our model vWF molecules to shear flow. In no-flow conditions, the assemble average $R_g = 9.264$ and standard deviation $\sigma = 1.97$. Relatively little fluctuations persist in the no-flow case, consistent with the vWF polymer forming a compact globule.

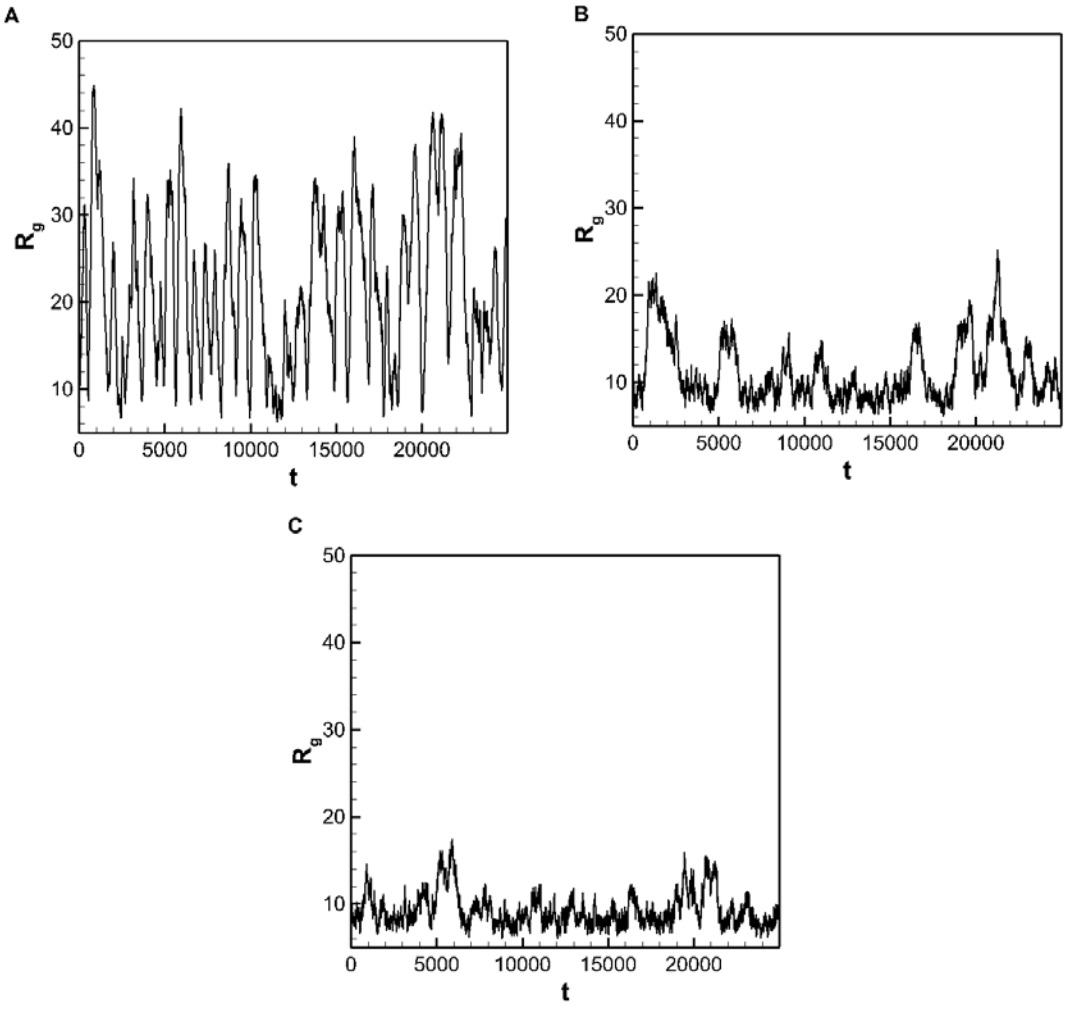

Fig. 3.2.5 Time dependence for a 60-bead chain: (A) $\boldsymbol{Wi = 10}$ case, (B) $\boldsymbol{Wi = 1}$ case and (C) no flow case.

In hydrodynamic interactions simulations, the diffusion tensor for the RPY description $\boldsymbol{D}$ and weighting factor $\boldsymbol{\sigma}$ are solved at every time-step. This introduces roughly a factor of

25 between the computational expense for HI simulations compared to FD simulations. It is thus critical to assess in which situations HI must be included and when it can be neglected. The conformational behavior of N = 20 vWF multimers are tested under various strength of shear flow and compared with the results in FD. As seen in Fig. 7, HI has little effect on the conformational changes of vWF multimers when Wi is below unity. This is because the disturbance of the solvent by the slow motion of beads is negligible. When Wi is greater than unity, the degree of unfolding for HI cases is always smaller than for FD cases. The reason is that beads hidden inside the protein globule are shielded from the flow and only a small fraction of the beads experience the full drag force. A shield effect predicting HI plays a hindering role to unfolding was previously described. [64] Results here lend evidence to this observation and show the same conclusion can be made even though the details of the molecular model are different.

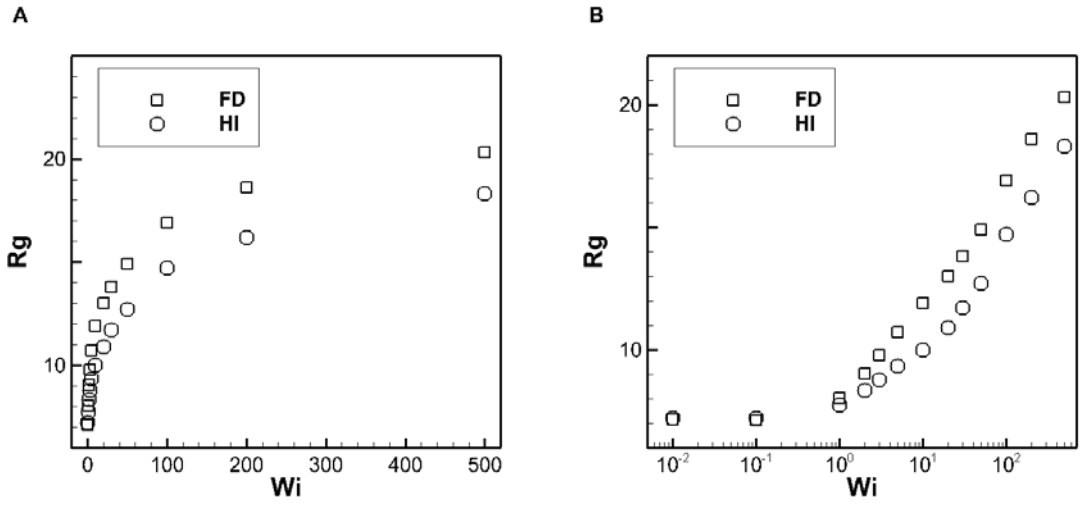

Fig. 3.2.6 Dependence of the radius-of-gyration $\boldsymbol{R_g}$ for 20 beads vWF chains on Weissenberg number ($\boldsymbol{Wi}$) for HI and FD cases: (A) linear scale plot and (B) log scale plot.

3.2.3 Calculation of intra-monomer domain response during flow

Results presented thus far underscore that the current model predicts multimer response to flow in very good agreement with prior simulations as well as available experimental data. A capability of the model presented is to simulate intra-monomer dynamics in terms of the elongational response of the FENE springs (i.e. the model A2 domains) to flow rate. Data in Fig. 8 show the ensemble average length of FENE springs in the FD case as a function of *Wi* as well as *N*. For $Wi < 10$, the model A2 domains remain at a length equal to that expressed at zero flow, which – in conjunction with adjacent beads – corresponds in real units to a monomer size near 40 *nm*. For $Wi > 10$, model A2 domain length increases with flow rate; at the highest *Wi* explored, the average value has nearly doubled or more, depending on *N*. Contrary to observations made from data in Fig. 5 for R_g versus *Wi*, data in Fig. 8 show that the dependence of the FENE spring length on *Wi* is stronger for smaller *N*. We explain this perhaps non-intuitive result in terms of data in Fig. 5. Larger molecules possess more modes of dynamic structural response through which they interact with a flow field; this is why larger molecules exhibit greater *N* dependence for molecular extension in high flow. Due to increased energy dissipation by molecular scale motion, less energy is dissipated by modes internal to the monomers. Thus, the dependence on *Wi* of the model A2 domain length is somewhat less for larger *N*.

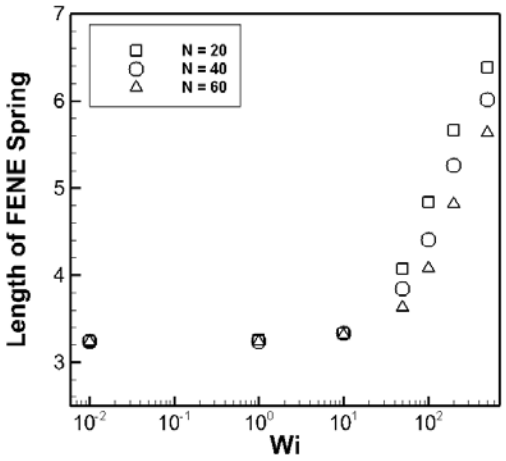

Fig. 3.2.7 Dependence of the Length of FENE spring for different length of chains on Weissenberg number (***Wi***).

The model unfolding transition for the A2 domain occurs near *Wi* = 10 whereas, for this model and prior similar models [20], multimer unfolding occurs for flow greater than *Wi* = 1. This order of magnitude increase for intra-monomer domain unfolding is likely reflective of a smaller relaxation time for FENE springs compared to the relaxation time for the multimer; the latter was the value used in computing *Wi* in Fig. 8. We did not attempt to compute a relaxation time for the FENE spring alone; however, supporting evidence for a significantly lower relaxation time is discussed below in regard to fluctuation dynamics for FENE springs in high flow. The overarching conclusion is that, as flow increases, the current model predicts a molecular unfolding transition that emerges at lower flow rate than a sub-monomer domain unfolding transition at higher flow rate.

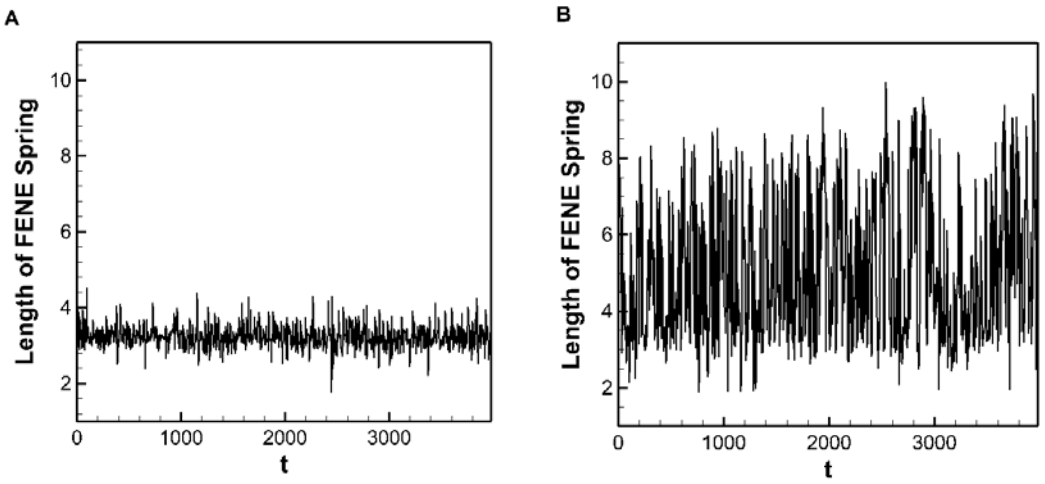

Fig. 3.2.8 Time dependence of the length of FENE spring for a 20-bead chain: (A) $\boldsymbol{Wi = 0}$ case, (B) $\boldsymbol{Wi = 100}$ case.

Similar to data shown in Fig. 6 for the time dependence of R_g at multiple flow rates, Fig. 9 shows analogous data for the FENE chain length time dependence. In this case, data are only shown for zero flow and *Wi* = 100 and, for the latter, significant fluctuations are manifest in the model A2 domain dynamics. Indeed, there are periodic excursions where the model A2 domain becomes nearly completely unfolded. As mentioned above, the fluctuation period observed in Fig. 9 is significantly smaller than that observed in Fig. 6; this supports the notion that FENE springs exhibit a significantly lower relaxation time than multimers. In accord with the model domain unfolding transition occurring near *Wi* = 10, significant fluctuations in the FENE spring dynamics do not emerge until above this transition as well. Data are only shown for *N* = 20; however, this analysis was done for all cases studied. Similar to the average FENE spring data, fluctuations in FENE spring length decrease somewhat with increasing *N*. However, this effect is small and all cases studied exhibited periodic excursions to nearly complete unfolding of the model A2 domain in high flow scenarios. The effect of HI on intra-monomer dynamics was

explored for $N = 20$ and it was found for that case that the inclusion of HI had negligible effects on intra-monomer dynamics. It remains possible that HI may have greater effect on the behavior of the model A2 domains for larger N and this will be a focus of future work.

Results here demonstrate the power of the current model in revealing not only multimer response to flow, but also intra-monomer domain response to flow. One role of the A2 domain is to interact with the ADAMTS13 enzyme to achieve scission of, in particular, ultra large vWF multimers in blood. The site in the A2 domain at which proteolysis occurs is shielded from the enzyme when multimers are in a compact globule conformation. For all cases studied here, the model A2 domains exhibit periodic complete unfolding at high flow rate; such behavior would abet interaction with ADAMTS13, leading to scission. Though larger N here was seen to result in a smaller dependence of the model A2 domain extension on flow, the dependence on N was relatively small. This was particularly true with regard to fluctuations. Furthermore, larger N means that a larger number of A2 domains are undergoing observed periodic complete expansion. Thus, for larger N, the likelihood for interaction between the A2 domain and ADAMTS13 is higher because more A2 domains are being exposed. Evidence here further suggests that those domains are also periodically expressing significant unfolding in high flow rate scenarios.

3.3 Conclusion

Brownian dynamics simulations using the novel vWF model presented in Chapter II have been performed to calculate the longest relaxation time τ of vWF multimers with different length in both FD and HI cases. The results revealed that the relaxation time

with HI is smaller than without HI for the same number of beads. A power-law scaling of relaxation time with number of beads exists, with exponents of 1.44 and 1.97 in simulations with and without HI, which agree well with predictions of the Rouse and Zimm models. The new model was used to study the conformational changes under various intensity of shear flow for vWF multimers. Molecular length has a profound influence on characteristics of vWF multimer under flow. Longer vWF chains have been proven to have more potential to unfold; this tendency becomes increasingly apparent for higher flows but only above the critical Weissenburg number of unity. This observation helps explain some of the observed dependence of vWF functionality on molecular size. The comparison of results with and without HI revealed that HI effect hinders unfolding of vWF multimers; thus, including HI is critical for modeling flow-induced conformational changes of vWF multimers.

Many of the conclusions reached in the current work are in accord with prior observations advanced in the literature. A unique feature of the current model is the ability to examine intra-monomer A2 domain unfolding dynamics. For flow rate about one order of magnitude higher than was necessary to achieve multimer unfolding, model A2 domain unfolding was observed. This difference in Wi at which unfolding was observed was explained in terms of relevant relaxation times on the two scales. For all cases studied and for Wi > 10, model A2 domains periodically adopted fully unfolded conformations. Thus, work here supports the notion that ultra large vWF secreted into the blood undergo scission partly as a result of A2 domain unfolding.

Work here represents an important step toward building new coarse grain molecular models that possess greater architectural complexity – as motivated by appropriate experimental observations. Here, the single molecule force spectroscopy presented in Ref. [15] provided quantitative information for parameterizing an entity to represent a sub-monomer domain that can unfold. Experimental observations of molecular size and structure guided development of other model parameters. As new experimental data are advanced – from AFM techniques, optical tweezer techniques, microfluidic flow methods, fluorescence microscopy analysis, and others – there exists an outstanding opportunity to develop coarse grain models capable of incorporating such data directly. The current model is under further development in order to quantitatively capture the already observed finite force of elongation onset that was observed for the A2 domain. Model development will also connect with experiments revealing details about the interaction between A3 domains in the vWF monomer and collagen. Such work will be crucial in developing quantitative reactive models capable of predicting molecular adhesion to tissue surfaces, platelet capture, and subsequent blood clotting behavior. Future work will couple our model to experimental studies necessary to achieve a thorough understanding of the physical mechanisms that bind vWF in different conformations to damaged vessel walls. An improved simulation model will be advanced that possesses the mechanical properties of the A2 domain illustrated here as well as experimentally parameterized monomer-collagen interactions. Our over-arching goal is to develop models possessing relative simplicity that can nonetheless help to understand the molecular mechanisms underlying vWF functionality as well as causes of vWF related

diseases (e.g. vWD and TTP). The hope underlying this goal is that such a model could provide important contributions for disease diagnosis and therapeutics.

Chapter 4 Homopolymers near a surface

4.1 Introduction

In the context of vWF adhesion, the single-chain behavior in an infinite medium represents just a single aspect of the process through which the molecule proceeds from a globular protein to an elongated molecule that is adsorbed to the surface of the blood vessel. [18,21] Therefore, another level of complexity has been be added in the polymer study by many researchers – the presence of surface. The behavior of vWF multimers in *vitro* exhibits increased potential for adhesion at high shear rate. Considering that most common polymers detach from surfaces at high shear rate, the adhesion of vWF multimers is counterintuitive. [18] Ma H.B has developed a continuum theory and showed common polymers would migrate away from the wall in shear flow because of hydrodynamic interactions between the chains and the wall. The depletion layer will be formed, which is determined by the normal stresses that develop in flow. [32] R.R. Netz used Brownian hydrodynamic simulations to investigate polymers adsorption. He concluded that shear flow weakens the adsorption of flexible polymers by hydrodynamic lift and surface friction due to surface potential corrugation weakens the surface attraction as well. [33] C.E. Sing found the hydrodynamic lift force displays a non-monotonic character, which increases linearly with the distance to the wall in near-surface regime and decays quadratically with the distance to the wall in far field. [35] Furthermore, S. Dutta et al. developed a kinetic theory incorporating bead-wall hydrodynamic interactions to investigate adsorption of homopolymers to a planar wall. They concluded shear flow causes migration of dumbbells and leads to desorption. Increasing the flow strength results in deceases of the quantity adsorbed and the film thickness. [27,28] These

research results clearly showed shear flow induced desorption of common polymers and are not sufficient to explain the observed vWF adsorption process.

Nonetheless, some breakthroughs have been made that help us to better elucidate how exactly vWF multimers adhere to the damaged vessel wall. Several interesting results pertaining to vWF multimer adsorption in shear flow were revealed in experimental performed by Schneider et al. [21] They found vWF multimers have significant conformational unfolding at shear rate above $5{,}000\ s^{-1}$ and the rate of adhesion as a function of shear rate precisely follows the jump in protein length. Based on the experimental facts that the unfolding and the adhesion of vWF multimers are concurrently happening, they concluded that vWF multimers adhesion on a collagen-coated surface is triggered by its conformation. Subsequent studies by Sing introduced Bell-model-type interaction to mimic the interaction between vWF multimer's A3 domain and collagen in simulation. [23] They found that shear-induced adsorption only occurs if the vWF-collagen bonds are slip-resistant such that force-induced unbinding is suppressed. Their simulation results quantitatively match Schneider's experimental observations. Then R.R. Netz investigated adsorption behavior of collapsed homopolymer on different surface models. The surface models are distinguished into three types: homogenous adsorbing surface, homogenous surface with a stagnant boundary layer and inhomogeneous surface consisting of discrete binding sites. The globule adsorptions for both cases are not enhanced by the presence of shear. They concluded a more complex binding mechanism is needed to explain the vWF adhesion behavior. [66] These studies apparently showed the presence of pure surface, which is represented by Lennard-Jones model, is not sufficient to investigate the physics

underlying the behavior exhibited by vWF both in *vitro* and in *vivo*. In order to resolve these apparent contradictions between vWF and fundamental polymer theory, we turn to add long time-scale binding behaviors between A3 domain and extracellular matrix collagens on the surface, represented by Bell model interactions.

4.2 Model descriptions

A vWF model employed here has been used by the present authors in a previous research. [67] The vWF model attempts to more realistically describe molecular architecture inherent in the protein. This is accomplished by modeling vWF monomers as a highly flexible A2 domain with relatively very rigid domains on either side of A2. The A2 domain, which has been shown to undergo significant unfolding during single molecule stretching experiments, is modeled as a finitely extensible nonlinear elastic (FENE) spring capable of significant extension; at each end of the spring is a spherical bead to represent neighboring rigid domains. Adjacent monomers are connected by a harmonic spring successively to form vWF multimers of desired length. We extend our previous research further from investigating unfolding of vWF multimer to studying adhesion of vWF multimer by adding a collagen-coated surface to the vWF model. Collagens that represent majority of the total protein of the vessel wall have been demonstrated to play a key role in binding with vWF. [68–70] Located underlying vascular endothelial cells, collagens are not exposed to blood flow. However, blood will flow over subendothelial structures including connective tissue that contains a high percentage of collagen after injury. Then vWF multimer combined with platelet adhere and bind to exposed collagens. The binding site involving in vWF binding to collagens is located in the A3 domain. So collagens coated on the surface can only interact with one bead of each vWF monomer in

our vWF model. A3 domain and collagen interactions are represented by reversible ligand-receptor-type bonds based on bell model kinetics. [23,37–39] Surface corrugation is not considered in this study and bonds are set in no-slip limit to counteract the lift force induced desorption, based on the prediction by Ref [23]. Model parameters controlling interaction strength and structural size are fit to reproduce experimentally observed data. The spring constant and the maximum extended length for the FENE spring are measured based on A2 domain force-extension experimental data. [15] The energy and length parameters for Lennard-Jones potential are optimized to mimic coiled vWF globule in poor solvent without flow. The activation energies of binding and unbinding, which control the probabilities of binding and unbinding between A3 domain of vWF multimer and collagen, were measured experimentally by force spectroscopy and were extracted using the Dudko-Hummer-Szabo model under different temperatures. [26,39] The density of collagens coated on the surface is roughly estimated by the concentration of collagens using in experiments.

4.3 Characteristics of von Willebrand Factor multimer adhesion

Characteristics of vWF adhesion have been investigated for two cases: free draining (FD) case in the limit without the presence of hydrodynamic interactions and with the presence of hydrodynamic interactions (HI) case. Fig. 2 shows the time evolution of 20 beads vWF multimers in FD for $Wi = 40$. Two polymer chains have different initial configurations and the HI effect is not considered in these simulations. vWF multimers move cyclically with constant unfolding and refolding when they are not interacting with collagens, as shown in Fig. 2. Typical unfolding stages are shown in Fig. 2 (i) A and (ii) A and coiled stages are shown in Fig. (i) B and (ii) B. Chains are pulled toward the

surface gradually and the bond between A3 domain and collagen may form when the distance between the bead that contains A3 domain and collagen is smaller than the reaction radius $\tilde{q}$. As we can see in Fig. 2 (i) C and (ii) C, four monomers react with collagens in each vWF multimer. Because of high activation energy of unbinding, the reversible process to break the bond between A3 domain and collagen is difficult. It makes vWF multimers anchoring on the surface once collagens actively react with the segment of the vWF multimers. Since the mobility of the vWF now is limited, the fluctuation in Rg is reduced significantly. When vWF multimers have little or no interaction with collagens vWF switching between folding and unfolding states, as manifested with large amplitude fluctuating in R_g. The difference between these two vWF multimers shown in Fig. 2 (i and ii) is that the vWF multimer in binding state in Fig. 2 (ii) is unfolded more than the vWF multimer shown in Fig. 2 (i). vWF multimer shown in Fig. 2 (i) is coiled when it adheres to the collagen coated surface and it maintains the coiled configuration afterwards. The configuration difference demonstrates that the timing when adhesions happen is critical, which dictates the configuration of vWF multimers afterwards. The hydrodynamic interactions case has the same pattern as the DF cases showed in Fig. 2.

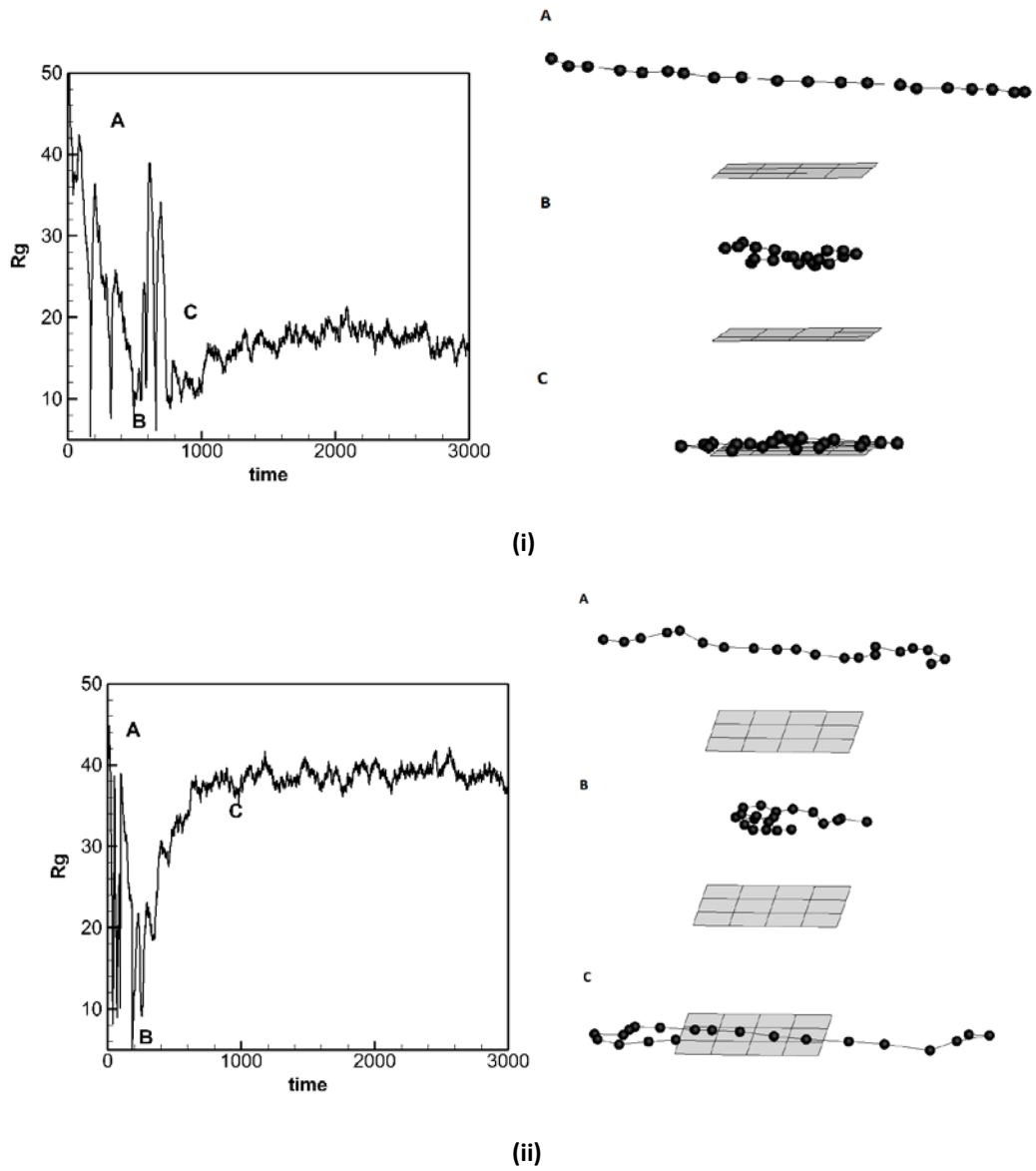

Fig. 4.3.1 Rg is plotted as a function of time for a 20-beads chain without HI when $\boldsymbol{Wi = 40}$ for two different initial configuration of vWF: (i) and (ii). Snapshots of polymer configuration are illustrated for various stages of vWF interactions with the wall: A. elongation; B. coiled and C. adhesion.

The probability distribution of radius-of-gyration R_g's ensemble average for a 20-beads chain without HI is shown in Fig. 3. The histogram is the results showing the behaviors of 100 vWF chains with different initial random seeds. As we can see, the distribution is shifting from left to right when the strength of shear flow increases, which means the chance that the vWF chain is unfolded when the adhesion happens increases. Generally,

the distributions represent what percentage of time that the certain conformations of vWF multimers occupy before the vWF multimers adhere to the surface.

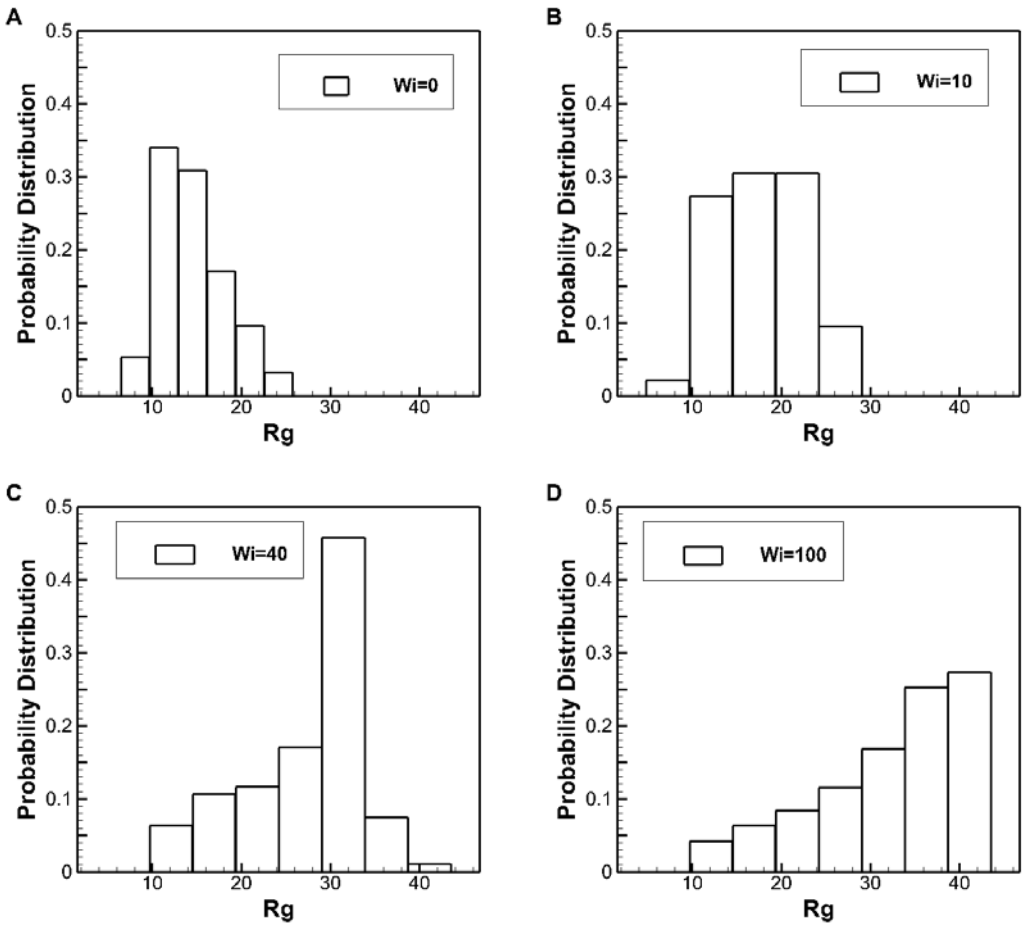

Fig. 4.3.2 Probability distribution of $\boldsymbol{R_g}$ for a 20-beads chain without HI: (A) no flow; (B) $\boldsymbol{Wi = 10}$; (C) $\boldsymbol{Wi = 40}$ and (D) $\boldsymbol{Wi = 100}$.

Fig. 4 shows the dependence of radius-of-gyration R_g on the length of vWF multimer in a no-flow condition without and with the presence of wall. It is found that R_g without the presence of wall scales as $N^{0.322}$, which is close to the exponent of power law in poor solvent. This implies that the vWF multimers are in globule state in the quiescent condition without the presence of the wall. The presence of a collagen-coated surface will make vWF multimers elongated and as a result it will make the exponent of power law to

be increased. This is illustrated in R_g vs N results shown below as the exponent is increased to 0.575.

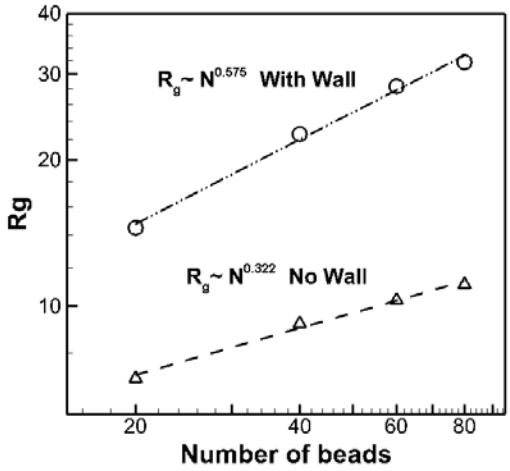

Fig. 4.3.3 Dependence of the radius-of-gyration $\mathbf{R_g}$ on the number of beads for wall cases and no-wall cases.

Fig. 5 shows the ensemble average of radius-of-gyration R_g as a function of Wi for four cases: free draining case near the collagen coated wall, free draining case in bulk, hydrodynamic interactions case near the collagen coated wall, and hydrodynamic interactions case in bulk. The R_g is averaged over the data of 32 different initialized chains after they have reached equilibrium. As expected, R_g monotonically increases with Wi and then approaches an apparent asymptote for all cases. As we can see in Fig. 5, the presence of the collagen-coated surface greatly influence the configuration of vWF multimers. Comparing the results between FD near the coated wall and FD in bulk and between HI near coated wall and HI in bulk, the R_g of vWF when it is near the wall is larger than the R_g of vWF away from coated surfaces at a given Wi. This demonstrates

that the adsorbed vWF multimers are more stretched than equivalent ones in bulk under the same flow condition. [24,46] Comparing these results, it is noted that the HI has effects on the conformational changes of vWF multimers with or without the presence of collagen-coated wall. Generally, the vWF multimers without HI effect are comparatively more stretched than the ones with HI effect. The reason is that the beads hidden inside the protein are shielded from the flow and only a small fraction of the beads experience the fully drag force. A HI shield beads and results in a hindering of unfolding of polymer chain. When HI is present a much stronger intensity of shearing is required to unfold vWF, as documented by the present authors. [64] It is also noted that HI has more profound effects of hindering of vWF without the presence of collagen-coated wall, as shown in Fig. 5.

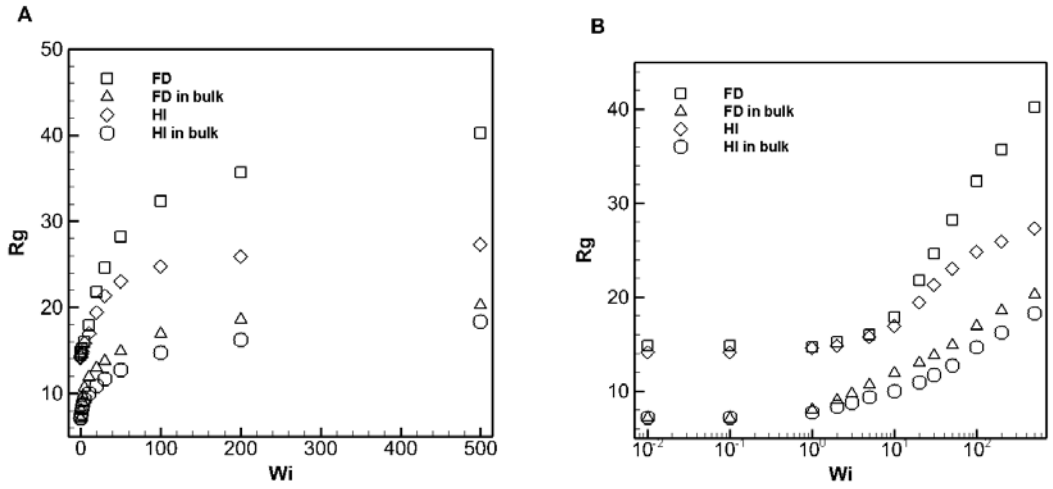

Fig. 4.3.4 Dependence of the radius-of-gyration $\boldsymbol{R_g}$ on Weissenberg number ($\boldsymbol{Wi}$) for four cases: free draining case; free draining in bulk case; hydrodynamic interactions case; and hydrodynamic interactions in bulk case. (a) linear scale plot and (b) log scale plot.

A capability of the model presented is to simulate intra-monomer dynamics in terms of the elongational response of the FENE springs (i.e. the model A2 domains). Data in Fig.

6 show the ensemble average length of FENE springs in the FD case as a function of Wi for four cases: free draining case; free draining in bulk case; hydrodynamic interactions case; and hydrodynamic interactions in bulk case. The length of FENE springs are averaged over the data of 320 FENE springs, considering there is 32 different initialized chains, each of which has 10 FENE springs. Comparing the results between FD near the coated wall and FD in bulk and between HI near coated wall and HI in bulk, the presence of the wall greatly elongates FENE springs i.e. the model A2 domains, which demonstrates the presence of the coated wall has a profound effect on intra-monomer behaviors. As we can see, there is little difference between the results of HI in bulk and FD in bulk, proving the effect of HI on intra-monomer behaviors is 3 without the coated wall. Comparing the results between FD near the coated wall and HI near the coated wall, there is little difference when $Wi < 10$. For $Wi > 10$, the model A2 domain length for both cases increases with flow rate and the rate of elongation of A2 domain for FD near the coated wall is larger than the one for HI near the coated wall. The reason as we can see in Fig. 7 is the difference of the adhesion rate for these two cases.

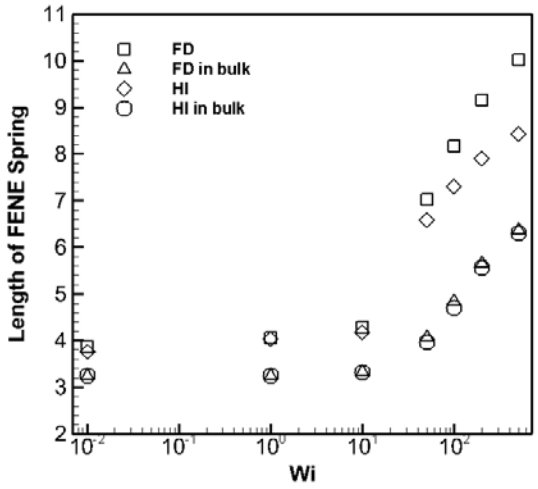

Fig. 4.3.5 Dependence of the Length of FENE spring on Weissenberg number (***Wi***) for four cases: free draining case; free draining in bulk case; hydrodynamic interactions case; and hydrodynamic interactions in bulk case.

The adhesion rate versus Wi for FD and HI cases are shown in Fig. 7. The adhesion rate is calculated by the fraction of the monomers in vWF multimers that have reacted with collagens and adhere to the surface. As shown in Fig. 7, the strength of shear flow has little influence on the adhesion rate in FD, but it has a strong influence when HI is included. As the strength of shear flow increases, the adhesion rate for HI case decreases significantly. In other words, the quantity of the adsorbed vWF multimers decreases with an increase in strength of shear flow. The different trends of adhesion rate versus Wi for FD case and HI case demonstrate the so-called hydrodynamic lift caused by the hydrodynamic interactions between surface and chains, which has been studied by many researchers. [27–36] In this study, the adhesion rate for HI case is determined from the balance between chains-wall attraction caused by bead-wall Lennard-Jones potential and HI-induced migration.

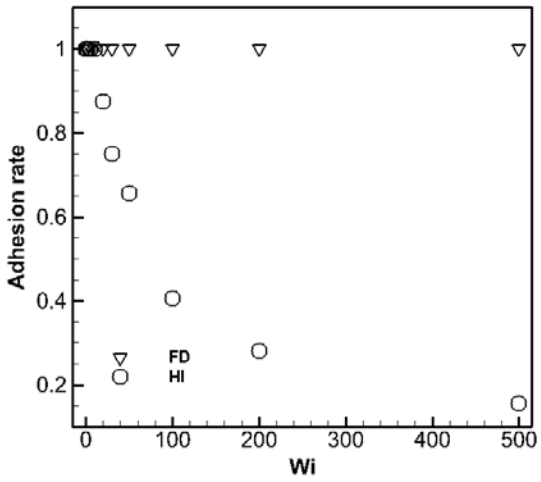

Fig. 4.3.6 Adhesion rate versus Weissenberg number ($\boldsymbol{Wi}$) for FD case and HI case.

The expected value of number of binding sites is calculated based on the probability distribution of number of binding sites during the total considered in the simulation for the whole vWF multimers. vWF multimers that migrate from the surface and have no reaction with collagens are not counted. The number of binding sites is ranging from 0 to 10 because the vWF multimer considered in this study has 10 monomers. As seen in Fig. 8, the number of binding sites is 4.16 for FD case and 4.13 for HI case in no flow condition and decrease to 1.89 for FD case and 1.27 for HI when $Wi = 500$. It is noticeable that the number of binding sites deceases with an increase in strength of shear flow and the vWF multimers with HI has fewer number of binding sites compared with the one without HI. It is concluded that the flow and HI impede the binding process between A3 domain and collagen. Once the vWF multimers adhere to the collagen coated surface, the tight bond will fasten the chains and distance between the center-of-mass of chains and the surface is 3.48 ± 0.02 no matter what the flow strength is and whether there is hydrodynamic interactions.

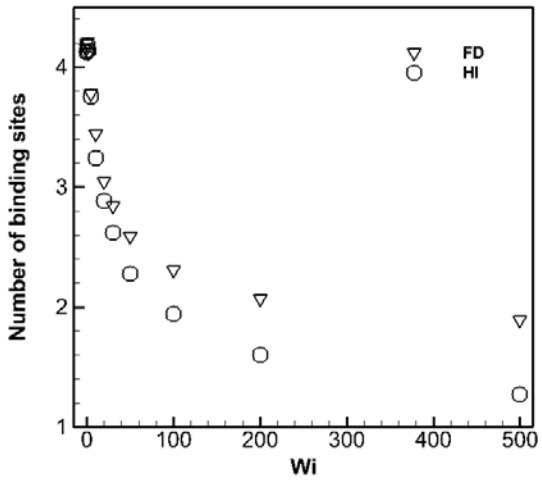

Fig. 4.7 The expected value of number of binding sites versus Weissenberg number ($\boldsymbol{Wi}$) for FD case and HI case.

4.4 Conclusions

In conclusion, a vWF multimer and collagen coated surface model has been introduced. The A2 domain in the present model is treated as a FENE spring with significant extensibility. The rigid domains of each vWF monomer are treated as two beads attached to one another by the FENE spring. Adjacent monomers are connected by a harmonic spring between one bead on each monomer, thus forming vWF multimers. The spring constant and the maximum extended length for the FENE spring are measured based on A2 domain force-extension experimental data. The energy and length parameters for Lennard-Jones potential are optimized to mimic coiled vWF globule in poor solvent without flow. Collagens are distributed on the surface homogenously. The distance between each collagen is estimated by the concentration of collagens using in experiments. A3 domain and collagen interactions are represented by reversible ligand-

receptor-type bonds based on bell model kinetics. The activation energies of binding and unbinding of the bell model were measured experimentally by force spectroscopy and were extracted using the Dudko-Hummer-Szabo model under different temperature. The tight bond between A3 domain and collagen is represented by a harmonic spring with a large spring constant. Brownian dynamics simulations using this model have been performed to understand a single vWF multimer adhesion process in both free-draining (FD) and hydrodynamic interactions (HI) cases. Results show vWF multimer adhesion to the collagen coated surface changes the movement from dynamic state with constant unfolding and refolding to static state that vWF multimers anchor on the surface. The timing when adhesions happen is critical, which dictates the configuration of vWF multimers afterwards. The presence of the collagen-coated surface greatly increases the stretching of vWF multimers and the elongation of FENE springs. HI effect plays a hindering role in unfolding of vWF multimer and elongation of FENE springs; but its effect is negligible on the elongation of FENE spring without the coated wall. The adhesion process is greatly impeded by the chain-wall hydrodynamic interactions, which result in hydrodynamic lift leading to vWF multimer migration. The number of binding sites deceases with an increase in strength of flow and the HI effect also prevents formation of binding sites. Some discrepancies still exist between our results and the experimental results. Schneider pointed out that the adhesion happens only when shear rate is above the threshold and adhesion rate increases with an increase of shear rate, which are not predicted in this study. [21] This in turn suggestes to construct more complex model that captures the interaction between vWF multimer and collagen coated surface accurately and realistically. Our current model, which reflects the dynamic

conformation of vWF under shear and simple interaction between A3 domain and collagen, will still help to understand the molecular mechanisms underlying vWF functionality as well as causes of vWF related diseases (e.g. vWD and TTP). Such a model could provide important implications for disease diagnosis and therapeutics.

Chapter 5 Homopolymers in confined geometries

5.1 Introduction

In the previous chapter we introduced a collagen-coated surface model into the vWF model as a way to describe the adhesion behaviors of vWF multimers onto the extracellular matrix when a blood vessel is damaged. Here we extend our research further by considering the vWF adhesion in complex confined geometries. The dynamics of homopolymers during flow in confined geometries is important in fields ranging from enhanced oil recovery to coating processes to analytical and preparatory separation techniques. [71] Apart from their direct importance in applications, confined polymer serves as an archetype for the dynamics of other confined complex fluids such as suspensions and emulsions. It is important that the fundamental mechanisms that underlie transport in these systems be understood. [71]

In the context of computational simulation of polymer solution near boundaries, a pioneering work has been done by Shaqfeh et al. that they considered rigid fibres as a simple polymer across streamlines in a suspension under plan Poiseuille flow. They showed at steady state the fibres's center-of-mass distribution function shows a net migration of fibres away from the centre of the channel and towards the channel walls. Jendrejack et al. added Hydrodynamic Interactions effect into the consideration and studied the dynamics of genomic DNA in the dilute limit within square microchannels of various sizes. They determined the Green's function numerically using a finite-element method. This approach granted them the capability to consider Hydrodynamic Interactions in the complex geometries. The results show that polymer chains migrate

away from the confining surfaces due to the hydrodynamic interactions between chains and walls. [72–74] Another approach to include Hydrodynamic Interactions of complex confinement into Brownian dynamics simulations is proposed by Hernandez-Ortiz. [75,76] A Fourier-based N log N approach is used to calculate a Green's function formalism, which is proved to greatly decrease the computation time. It splits point forces into a local contribution for which rapidly decaying free-space solution are used, and a global contribution whose effect is determined using fast iterative method. The effects of hydrodynamically induced migration phenomena are illustrated also. Around the same time, Fedosov et al. employed dissipative particle dynamics to study depletion and migration in dilute polymer solutions, in channels several times larger than the radius of gyration of bead-spring chains, for different chain models, solvent quality, and relative wall-solvent-polymer interactions. They found the center-of-mass distribution develops two symmetric off-center peaks, which identify the preferred chain positions across the channel.

5.2 Model description

The vWF in confined geometries model is revised directly from the one in chapter IV. The only difference is that the geometry of boundaries changes from a surface to a slit, which is accomplished by confining vWF multimers within two parallel collagen-coated surfaces. A3 domain of vWF and collagen interactions are represented by reversible ligand-receptor-type bonds based on bell model kinetics. [23,37–39] The energy and length parameters for Lennard-Jones potential are optimized to mimic coiled vWF globule in poor solvent without flow. The activation energies of binding and unbinding, which control the probabilities of binding and unbinding between A3 domain of vWF

multimer and collagen, were measured experimentally by force spectroscopy and were extracted using the Dudko-Hummer-Szabo model under different temperatures. [26,39] The density of collagens coated on the surface is roughly estimated by the concentration of collagens using in experiments.

5.3 Dynamics of vWF multimers within a collagen-coated slit

Brownian Dynamics (BD) simulations have bee used to study the dynamics of vWF multimers within a collagen-coated slit. The hydrodynamic interaction is excluded in this chapter and will be considered in further research. One issue arises in a confined polymer solution is that if the confinement has the same length scale as the polymer molecules themselves, and then the equilibrium conformations of the chains can be expected to change substantially from their bulk behavior. In a good solvent, confinement of the chain in one or two directions leads to expansion of the chain in the unconfined dimensions. When the solvent is in ideal conditions, the chain would be compressed in the confined directions, but the chain statistics in the unconfined directions would be unchanged.

In the weak confined regime, the equilibrium conformational statistics of the polymer chain are largely unchanged from bulk values. When the vWF multimers are set up in the middle of the slit under certain flow conditions no matter couette flow or Poiseuille flow, the chain will stay close to the center streamline and have no adhesion happening with the surfaces. When the chains are set up in one-quarter position of the gap, they will drift to the surface, which is close to them, and adhere to the surface because of the interactions between collagens and A3 domains. The conformation and dynamics of vWF multimers is similar to the case when there is only one surface.

Chapter 6 Conclusion

von Willebrand Factor is one of the initial responders in the blood clotting cascade, and acts as the intermediary that holds together the initial plug structure. [8,10,77] In the case of vessel walls exposed to low shear rates, the platelets adhere directly to the exposed extracellular matrix collagens. While at high shear rates, vWF becomes requisite because platelets no longer retain a sufficient level of adhesion at the surface to form blood clots. [8,10,78] In this case, vWF is known to act on a number of functional receptors: the A3 domain on vWF binds to collagen fibers at the surface of the extracellular matrix and vWF interact with platelets through the integrins and the glycoprotein GP1b. [6,8] The combination of these interactions that make the initial thrombus possible. vWF has extremely complicated structure, largely due to these various domains. The molecule, in an unraveled state where repeat units can be envisioned to roughly line up, can span tens of microns. At a smaller length scale of order tens to one hundred nanometers are the individual repeat units; these monomers consist of a collection of folded domains, each with a specific chemical binding affinity. Thus, two scales of unfolded are considered in this dissertation: on the larger length scale is unfolding of the overall molecule as monomers become more lined up; on the smaller length scale is unfolding of individual domains. Specifically, Zhang, *et al.*, using single molecule force spectroscopy methods, showed the inner structure and mechanical characteristics of a vWF monomer's domains. [15] Their work pointed out that the A2 domain of vWF, which lacks protection by disulfide bonds, could be unfolded with applied forces that, though non-trivial, may indeed manifest under very rapid blood flow conditions. Furthermore, relative to the size of an unextended monomer, the A2 domain demonstrates a large degree of elongation via

unfolding. A novel vWF model attempts to more realistically describe molecular architecture inherent in the protein are presented in this dissertation. Specifically, the model captures aspects of what we believe to be a primary mechanical response of a single monomer, as well as adjacent monomer-monomer mechanics. This is accomplished by modeling vWF monomers as an extensible domain with relatively rigid domains on either side of it. The A2 domain has been shown to undergo significant unfolding during single molecule stretching experiments. [15] The extensible regions, or domains, on a vWF monomer are thus modeled as a FENE spring capable of significant extension. At each end of the spring is a spherical bead to represent neighboring rigid domains. Adjacent monomers are connected by a relatively stiff harmonic spring between a bead on each monomer, thus forming vWF multimers of desired length.

Applying this novel vWF model, the dissertation is aimed to investigate the physics underlying the behaviors exhibit by vWF both in *vitro* and in *vivo*. We started with a straightforward setup by considering a collapsed homopolymers in an infinite medium under the influence of fluid flow. The results revealed that the relaxation time with HI is smaller than without HI for the same number of beads. A power-law scaling of relaxation time with number of beads exists, with exponents of 1.44 and 1.97 in simulations with and without HI, which agree well with predictions of the Rouse and Zimm models. Molecular length has a profound influence on characteristics of vWF multimer under flow. Longer vWF chains have been proven to have more potential to unfold; this tendency becomes increasingly apparent for higher flows but only above the critical Weissenburg number of unity. This observation helps explain some of the observed dependence of vWF functionality on molecular size. The comparison of results with and

without HI revealed that HI effect hinders unfolding of vWF multimers; thus, including HI is critical for modeling flow-induced conformational changes of vWF multimers. The conclusions reached in the current work are in accord with prior observations advanced in the literature. A unique feature of the current model is the ability to examine intra-monomer A2 domain unfolding dynamics. For flow rate about one order of magnitude higher than was necessary to achieve multimer unfolding, model A2 domain unfolding was observed. This difference in Wi at which unfolding was observed was explained in terms of relevant relaxation times on the two scales. For all cases studied and for Wi > 10, model A2 domains periodically adopted fully unfolded conformations.

The dissertation is extended to the context of vWF adhesion by adding another level of complexity – the presence of collagen-coated surface. Collagens that represent majority of the total protein of the vessel wall have been demonstrated to play a key role in binding with vWF. [68–70] A3 domains on vWF and collagen interactions are represented by reversible ligand-receptor-type bonds based on bell model kinetics. [23,37–39] These bonds are set in no-slip limit to counteract the lift force induced desorption, based on the prediction by Ref [23]. Results show vWF multimer adhesion to the collagen-coated surface changes the movement from dynamic state with constant unfolding and refolding to static state that vWF multimers anchor on the surface. The timing when adhesions happen is critical, which dictates the configuration of vWF multimers afterwards. The presence of the collagen-coated surface greatly increases the stretching of vWF multimers and the elongation of FENE springs. HI effect plays a hindering role in unfolding of vWF multimer and elongation of FENE springs; but its effect is negligible on the elongation of FENE spring without the coated wall. The

adhesion process is greatly impeded by the chain-wall hydrodynamic interactions, which result in hydrodynamic lift leading to vWF multimer migration. The number of binding sites deceases with an increase in strength of flow and the HI effect also prevents formation of binding sites. The research results in this dissertation, which reflects the dynamic conformation of vWF under shear and simple interaction between A3 domain and collagen, will help to understand the molecular mechanisms underlying vWF functionality as well as causes of vWF related diseases (e.g. vWD and TTP) and provide important implications for disease diagnosis and therapeutics.

Appendix A: Hydrodynamic Interaction Diffusivity Tensor

The diffusivity tensor $\mathbf{D}$ has 3×3 block components, $\mathbf{D}_{ij}$ that are given by

$$\mathbf{D}_{ij} = \mathbf{\Omega}_{ij} + \delta_{ij}\mathbf{I} \tag{A1}$$

where $\mathbf{I}$ is the identity tensor, δ_{ij} is the Kronecker delta. In order to account for the finite bead size in the simulations, $\mathbf{\Omega}_{ij}$ is expressed as,

$$\mathbf{\Omega}_{ij} = \left(1 - \delta_{ij}\right)\mathbf{\Omega}^{RPY}(\mathbf{r}_i, \mathbf{r}_j) + \mathbf{\Omega}^{W}(\mathbf{r}_i, \mathbf{r}_j) \tag{A2}$$

where $\mathbf{\Omega}^{RPY}(\mathbf{r}_i, \mathbf{r}_j)$ is the RPY mobility tensor, which has been mentioned previously, and $\mathbf{\Omega}^{W}(\mathbf{r}_i, \mathbf{r}_j)$ is a correction that accounts for the no-slip condition at the wall.

$$\mathbf{\Omega}^{W}\left(\mathbf{r}_i, \mathbf{r}_j\right) = \mathbf{\Omega}^{W}_{\mathrm{PF}}\left(\mathbf{r}_i, \mathbf{r}_j\right) - \frac{2a^2}{3}\mathbf{\Omega}^{W}_{\mathrm{c}}\left(\mathbf{r}_i, \mathbf{r}_j\right) \tag{A3}$$

where the second term on the right-hand side is a correction term that accounts for finite bead size. The expressions for $\mathbf{\Omega}^{W}_{\mathrm{c}}\left(\mathbf{r}_i, \mathbf{r}_j\right)$ and $\mathbf{\Omega}^{W}_{\mathrm{PF}}\left(\mathbf{r}_i, \mathbf{r}_j\right)$ are given below.

$$\mathbf{\Omega}^{W}_{\mathrm{c}}\left(\mathbf{r}_i, \mathbf{r}_j\right) = \frac{\mathbf{\Omega}^{W}_{\mathrm{PD}}(\mathbf{r}_i, \mathbf{r}_j) + \mathbf{\Omega}^{W}_{\mathrm{PD}}(\mathbf{r}_j, \mathbf{r}_i)^{T}}{2} \tag{A4}$$

$$\mathbf{\Omega}^{W}_{\mathrm{PF}}\left(\mathbf{r}_i, \mathbf{r}_j\right) = \frac{3a}{4}\left(-\mathbf{S}\left(\mathbf{r}_i - \mathbf{r}_j{}^{Im}\right) + 2z_0^2\mathbf{P}^{D}\left(\mathbf{r}_i - \mathbf{r}_j{}^{Im}\right) - 2z_0\mathbf{S}^{D}\left(\mathbf{r}_i - \mathbf{r}_j{}^{Im}\right)\right. \tag{A5}$$

where $\mathbf{r}_j{}^{Im}$ is the location of the image of the point force and z_0 is the perpendicular distance of the point force from the wall. The free-space Stokeslet is given by $\mathbf{S}$, $\mathbf{P}^{D}$ is the potential dipole, and $\mathbf{S}^{D}$ is the Stokeslet doublet.

$$S_{ij}(\mathbf{r}) = \frac{\delta_{ij}}{|\mathbf{r}|} + \frac{r_i r_j}{|\mathbf{r}|^3} \tag{A6}$$

$$P^{D}_{ij}(\mathbf{r}) = \pm\left(\frac{\delta_{ij}}{|\mathbf{r}|^3} - 3\frac{r_i r_j}{|\mathbf{r}|^5}\right) \tag{A7}$$

$$S^{D}_{ij}(\mathbf{r}) = r_3 P^{D}_{ij}(\mathbf{r}) \pm \frac{\delta_{j3} r_i - \delta_{i3} r_j}{|\mathbf{r}|^3} \tag{A8}$$

where the minus sign is for the direction normal to the wall ($j = 3$) and plus sign is for the planar directions ($j = 1$ and 2). The $\mathbf{\Omega}_{\mathrm{PD}}^{W}(\mathbf{r}_i, \mathbf{r}_j)$ is a correction to the free-space mobility tensor for a potential dipole to account for the no-slip and is given by

$$\mathbf{\Omega}_{\mathrm{PD}}^{W}(\mathbf{r}_i, \mathbf{r}_j) = \frac{3a}{4}\begin{bmatrix} H_{xx} & H_{xy} & H_{xz} \\ H_{yx} & H_{yy} & H_{yz} \\ H_{zx} & H_{zy} & H_{zz} \end{bmatrix} \tag{A9}$$

$$H_{xx} = \frac{1}{R_{ij}^3} - \frac{3x^2}{R_{ij}^5} - \frac{6z(z-z_j)}{R_{ij}^5} + \frac{30x^2z(z-z_j)}{R_{ij}^7} \tag{A10}$$

$$H_{xy} = H_{yx} = -\frac{3xy}{R_{ij}^5} + \frac{30xyz(z-z_j)}{R_{ij}^7} \tag{A11}$$

$$H_{xz} = \frac{x(9z-6z_j)}{R_{ij}^5} - \frac{30xz^2(z-z_j)}{R_{ij}^7} \tag{A12}$$

$$H_{yy} = \frac{1}{R_{ij}^3} - \frac{3y^2}{R_{ij}^5} - \frac{6z(z-z_j)}{R_{ij}^5} + \frac{30y^2z(z-z_j)}{R_{ij}^7} \tag{A13}$$

$$H_{yz} = \frac{y(9z-6z_j)}{R_{ij}^5} - \frac{30yz^2(z-z_j)}{R_{ij}^7} \tag{A14}$$

$$H_{zx} = -\frac{3x(z-2z_j)}{R_{ij}^5} + \frac{30xz^2(z-z_j)}{R_{ij}^7} \tag{A15}$$

$$H_{zy} = -\frac{3y(z-2z_j)}{R_{ij}^5} + \frac{30yz^2(z-z_j)}{R_{ij}^7} \tag{A16}$$

$$H_{zz} = \frac{1}{R_{ij}^3} + \frac{3z(5z-6z_j)}{R_{ij}^5} - \frac{30z^3(z-z_j)}{R_{ij}^7} \tag{A17}$$

in which x, y, z and are the components of the vector $\mathbf{r}_i - \mathbf{r}_j{}^{Im}$ and $R_{ij} = \left|\mathbf{r}_i - \mathbf{r}_j{}^{Im}\right|$.

Appendix B: Supporting materials for Chapter II

The relaxation curves for square of end-to-end distance versus time for N = 40 vWF multimers are shown in Fig. B1. As you can seen, the equilibrium value of $\langle R^2 \rangle$ i.e. $\langle R^2 \rangle_{eq}$ is neglected in the plots, because it has no influence on the curve-fitting. Clearly, the longest relaxation time is measured in regime where the ratio of end-to-end distance to L is less than 0.3. The reason for

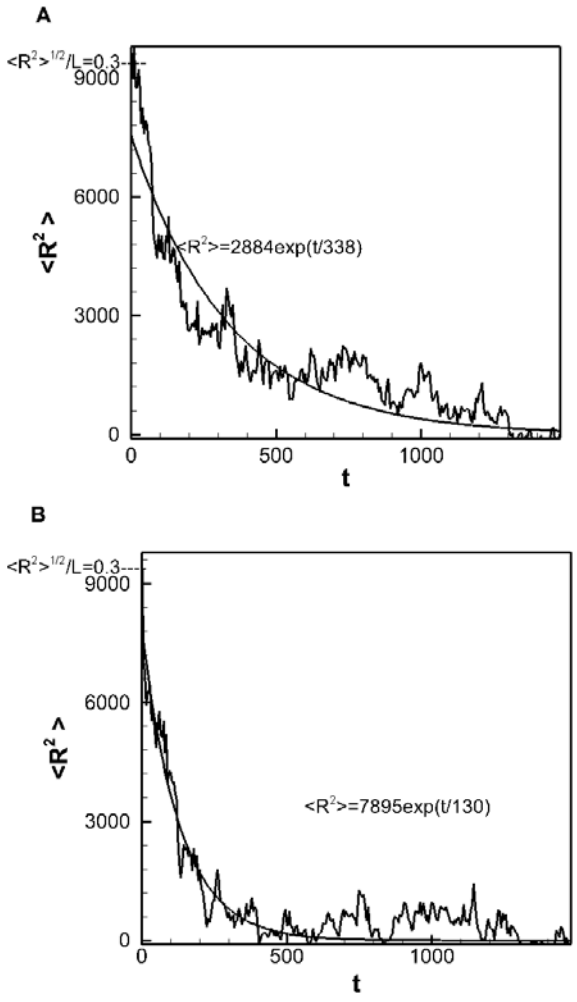

Fig. B 1 Relaxation curves for square of end to end distance versus time using 40 beads (A) without HI and (B) with HI.

fitting only for relatively small amounts of extension is that the contribution of higher order relaxation modes should be neglected. Clearly shown in Fig. B1, the N = 40 vWF multimer with HI is relaxing to a globule state faster than without HI.

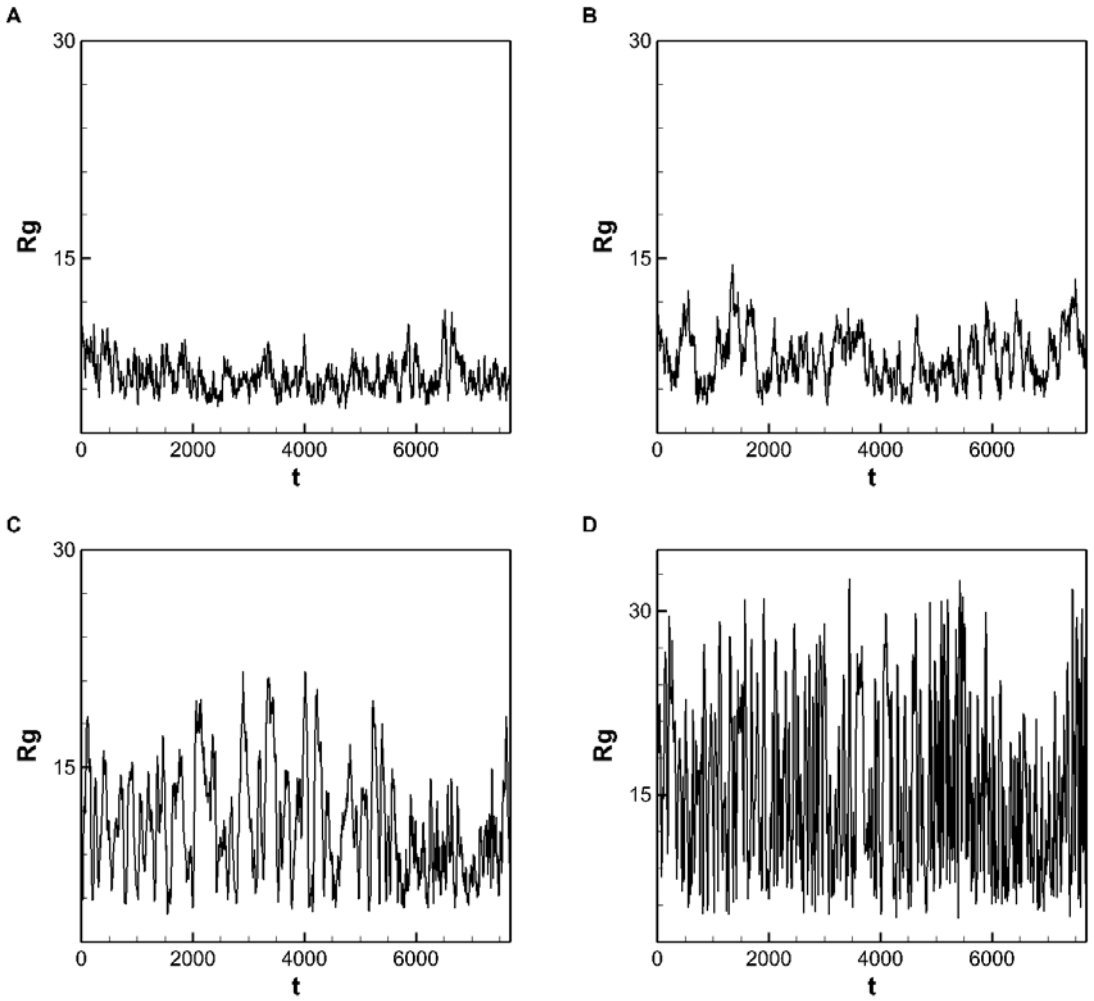

Fig. B 2 Time dependence for a 20-bead chain: (A) no flow case, (B) $\boldsymbol{Wi = 1}$ case, (C) $\boldsymbol{Wi = 10}$ case and (D) $\boldsymbol{Wi = 50}$ case.

Temporal characteristics for a single N = 20 vWF multimer under no flow condition and in $Wi = 1$, 10 and 50 shear flow are represented in Fig. B2. As we can see, there is little difference between no flow case and $Wi = 1$ case. The Fig. B2 (A) and (B) both show

few unfolding events and overall small fluctuations. As the Fig. B2 goes to (C) $Wi = 10$ case and (D) $Wi = 50$ case, the vWF multimer reacted rapidly to the shear flow such that there is no apparent transient state and is significantly uncoiled at some points, which can enable the A3 domain to bind to collagen.

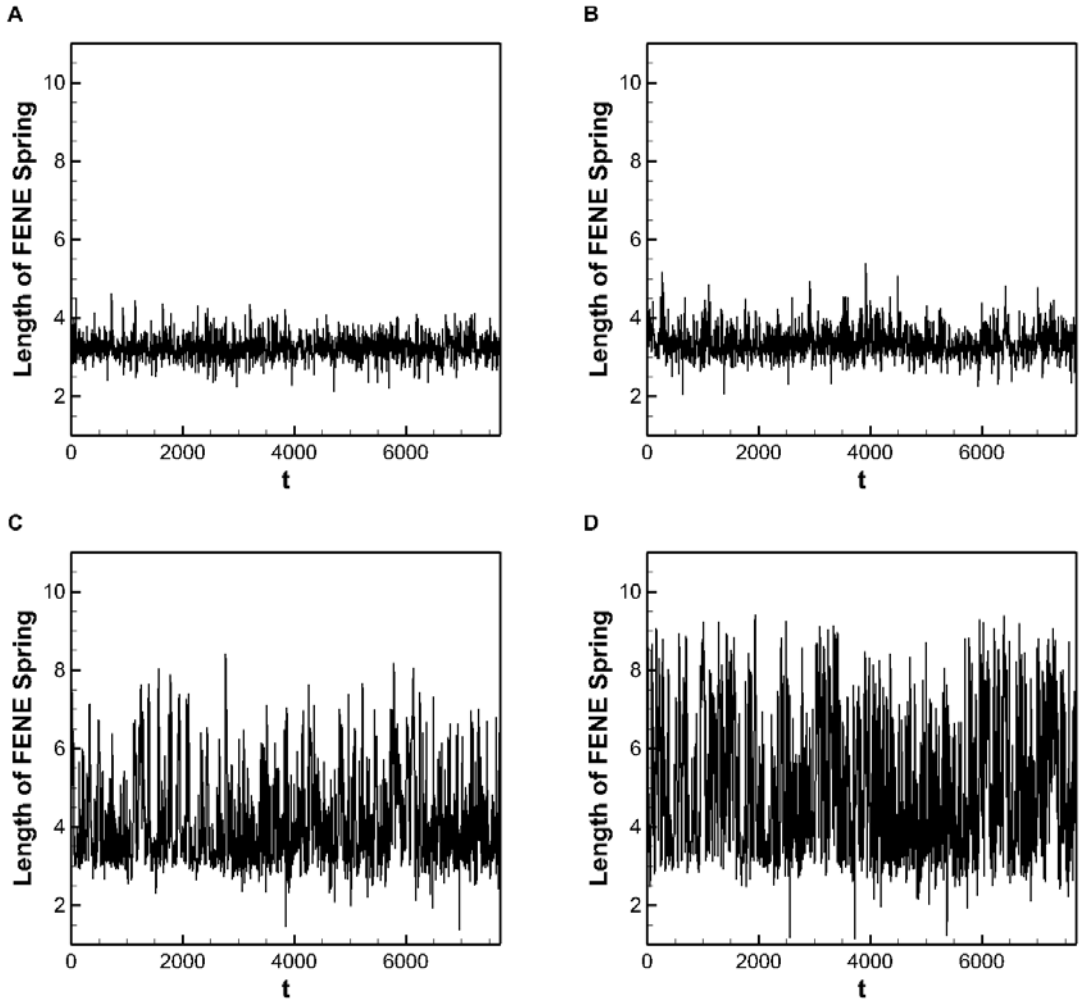

Fig. B 3 Time dependence of the length of FENE spring for a 20-bead chain: (A) $\boldsymbol{Wi = 1}$ case, (B) $\boldsymbol{Wi = 10}$ case, (C) $\boldsymbol{Wi = 50}$ case, (D) $\boldsymbol{Wi = 100}$ case.

Similar to data shown in Fig. B2 for the time dependence of R_g at multiple flow rates, Fig. B3 shows analogous data for the FENE chain length time dependence. Generally, the critical Weissenburg number Wi is above 10. As we can seen, there is few unfolding of

FENE springs and little fluctuation when Wi is below 10. Whereas, the Wi goes above 10 to 50 and even 100, the unfolding of FENE springs is becoming very frequently and strongly. As mentioned in Chapter II, the fluctuation period observed in Fig. B3 is significantly smaller than that observed in Fig. B2; this supports the notion that FENE springs exhibit a significantly lower relaxation time than multimers.

Appendix C: Supporting materials for Chapter III

Time evolutions of 20 beads vWF multimers with Hydrodynamic Interactions (Hi) for $Wi = 40$ are shown in Fig. C1. As we can see, there are three difference types when the simulations include HI effects: (A) the dynamic of vWF multimer has cycles of unfolding and refolding; (B) the dynamic of vWF multimer has cycles of unfolding and refolding and then changes to a static state; (C) the dynamic of vWF multimer keeps in the static state. The rationale behind these different patterns is that the vWF multimer in Fig. C1 (A) has no binding interaction with the collagen-coated surface and the surface imposes no restriction on the movement of the vWF multimer, which results in the unfolding and refolding movements close to the dynamic of vWF

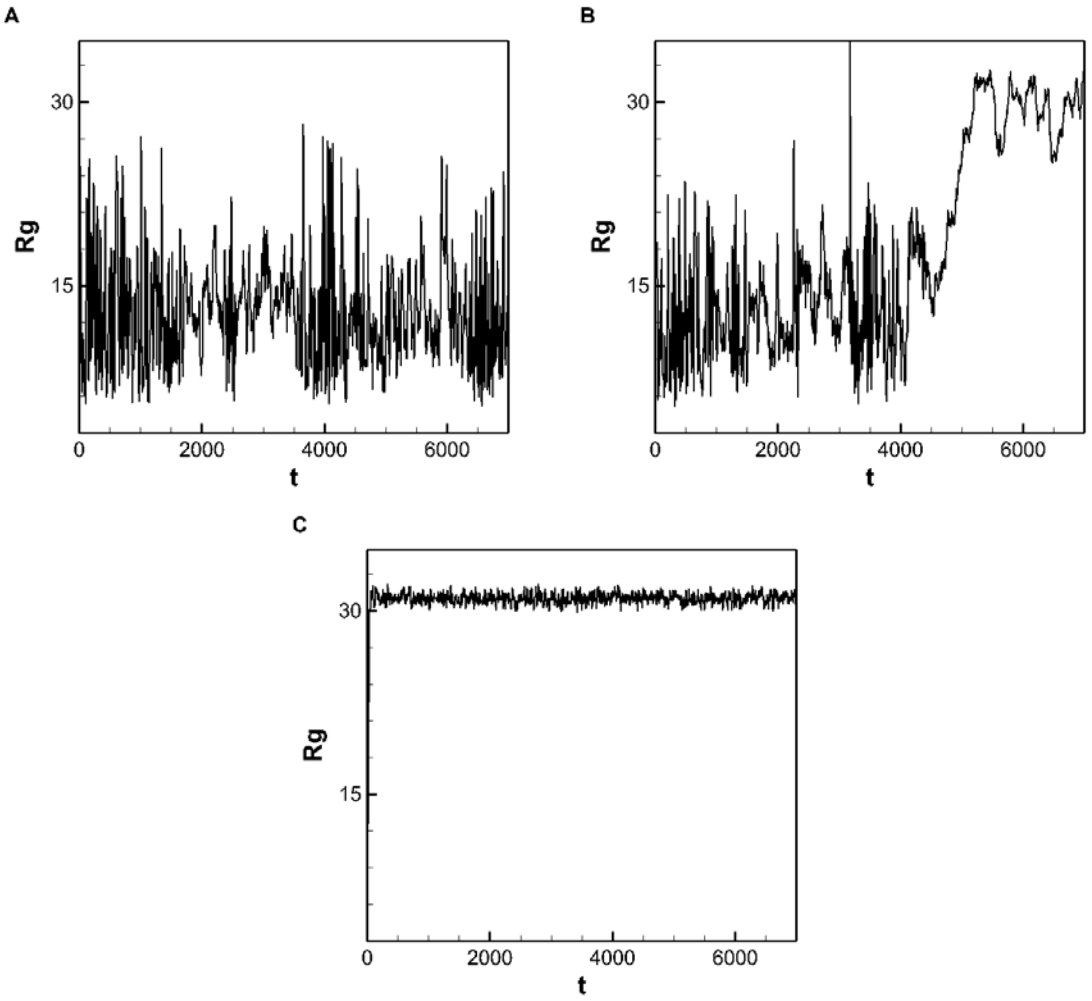

Fig. C 1 Time dependence for a 20-bead chain when $\boldsymbol{Wi = 40}$ with HI effect.

multimer without the surface. The pattern shown in Fig. C1 (C) has a dramatically fast increase in R_g and then reaches to equilibrium with few unfolding and little fluctuation, because the vWF multimer binds to the collagen-coated surface at the beginning of the simulation, which dictate the dynamic afterwards. The one shown in Fig. C1 (B) has both patterns of Fig. C1 (A) and Fig. C1 (C) mentioned above, because the binding happen at the middle of the process and the pattern at the first half is similar to the one in Fig. C1 (A); the pattern at the second half is similar to the one in Fig. C1 (C).

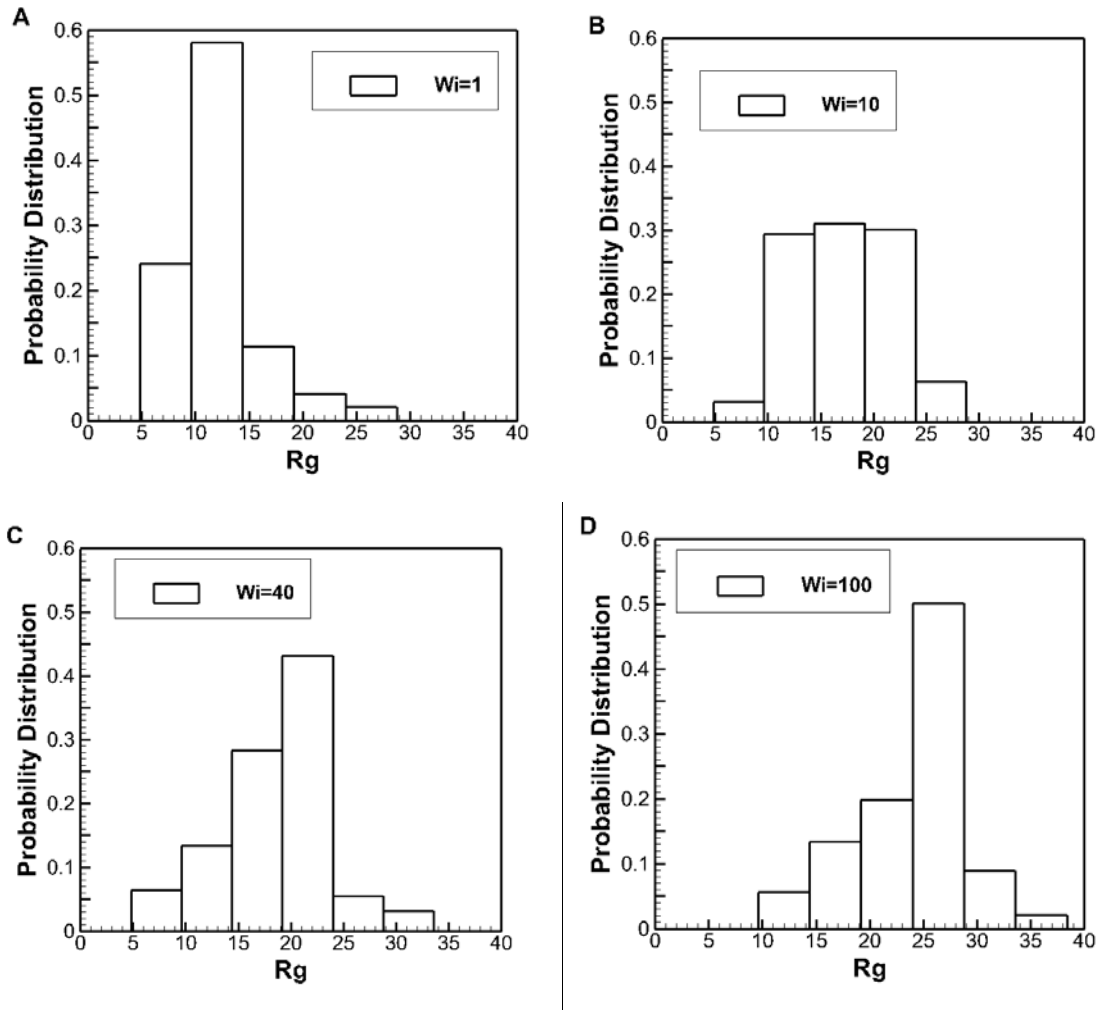

Fig. C 2 Probability distribution of $\boldsymbol{R_g}$ for a 20-beads chain with HI: (A) $\boldsymbol{Wi = 1}$; (B) $\boldsymbol{Wi = 10}$; (C) $\boldsymbol{Wi = 40}$ and (D) $\boldsymbol{Wi = 100}$.

The probability distribution of radius-of-gyration R_g's ensemble average for a 20-beads chain with HI is shown in Fig. C2. The histogram is the results showing the behaviors of 100 vWF chains with different initial random seeds. As we can see, the distribution is shifting from left to right when the strength of shear flow increases, which means the chance that the vWF chain is unfolded when the adhesion happens increases. Generally, the distributions represent what percentage of time that the certain conformations of vWF multimers occupy before the vWF multimers adhere to the surface.

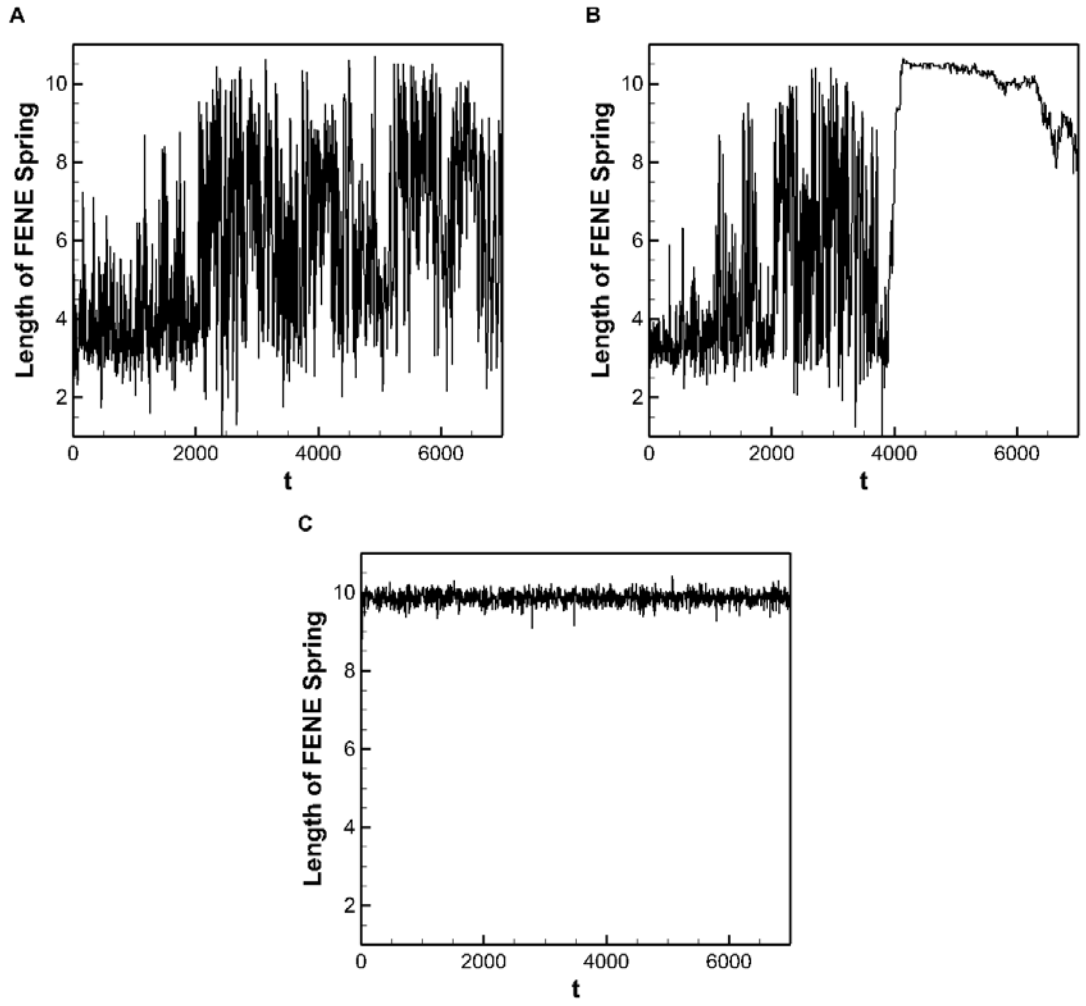

Fig. C 3 The length of three different FENE Springs in the same chain are plotted as a function of time with HI and for $\boldsymbol{Wi = 50}$.

A capability of the model presented is to simulate intra-monomer dynamics in terms of the elongational response of the FENE springs (i.e. the model A2 domains). The dynamics of three different FENE spings in the same chain are presented in Fig. C3. The FENE spring in Fig. C3 (A) is at one end of the chain, which is less elongated and has larger fluctuations, because adjacent beads did not anchor on the surface. However, the model A2 domain in Fig. C3 (C) is in a monomer at the middle of the chain; this spring is significantly more elongated and has smaller fluctuations, due to an adjacent bead (and other nearby beads) being bound to the surface. The FENE spring shown in Fig. C3 (B)

has the both patterns in Fig.C3 (A) and (C), because the binding between the adjacent beads happened at the middle of the simulation. It is interesting to note that the elongated model A2 domain is at nearly full extension in this condition. In the human body, part of the role played by this domain is that, once blood clotting has initiated, the species ADAMTS13 interacts with A2 domains to drive polymer scission at the site. This is a way that vWF essentially turns off its activity after its initial job is complete. Results here perhaps provide some insight into this mechanism in that it appears that A2 domains near bound positions are more likely to be in an elongated state.

Bibliography

[1] M.D. Wang, Manipulation of single molecules in biology., Curr. Opin. Biotechnol. 10 (1999) 81–6.

[2] L.H. Sperling, INTRODUCTION TO PHYSICAL POLYMER, n.d.

[3] A.F. Oberhauser, P.E. Marszalek, H.P. Erickson, J.M. Fernandez, The molecular elasticity of the extracellular matrix protein tenascin., Nature. 393 (1998) 181–185.

[4] L. Tskhovrebova, J. Trinick, J.A. Sleep, R.M. Simmons, Elasticity and unfolding of single molecules of the giant muscle protein titin., Nature. 387 (1997) 308–312.

[5] M. Rief, Reversible Unfolding of Individual Titin Immunoglobulin Domains by AFM, Science (80-.). 276 (1997) 1109–1112. doi:10.1126/science.276.5315.1109.

[6] S.F. De Meyer, B. De Maeyer, H. Deckmyn, K. Vanhoorelbeke, Von Willebrand factor: drug and drug target., Cardiovasc. Hematol. Disord. Drug Targets. 9 (2009) 9–20.

[7] J.E. Sadler, BIOCHEMISTRY AND GENETICS, (1998) 395–424.

[8] T.A. Springer, Review Article von Willebrand factor , Jedi knight of the bloodstream, 124 (2014) 1412–1425. doi:10.1182/blood-2014-05-378638.Helical.

[9] et al Nigel Key, Michael Makris, Practical Hemostasis and Thrombosis, 2009.

[10] Z.M. Ruggeri, Von Willebrand factor: looking back and looking forward., Thromb. Haemost. 98 (2007) 55–62. doi:10.1160/TH07.

[11] H.E. Gerritsen, R. Robles, B. La, Plenary paper Partial amino acid sequence of purified von Willebrand factor – cleaving protease, 98 (2001) 1654–1661.

[12] G.G. Levy, W.C. Nichols, E.C. Lian, T. Foroud, J.N. McClintick, B.M. McGee, et al., Mutations in a member of the ADAMTS gene family cause thrombotic thrombocytopenic purpura., Nature. 413 (2001) 488–94. doi:10.1038/35097008.

[13] K. Soejima, N. Mimura, M. Hirashima, H. Maeda, T. Hamamoto, T. Nakagaki, et al., A novel human metalloprotease synthesized in the liver and secreted into the blood: possibly, the von Willebrand factor-cleaving protease?, J. Biochem. 130 (2001) 475–80.

[14] X. Zheng, D. Chung, T.K. Takayama, E.M. Majerus, J.E. Sadler, K. Fujikawa, Structure of von Willebrand factor-cleaving protease (ADAMTS13), a metalloprotease involved in thrombotic thrombocytopenic purpura., J. Biol. Chem. 276 (2001) 41059–63. doi:10.1074/jbc.C100515200.

[15] X. Zhang, K. Halvorsen, C.-Z. Zhang, W.P. Wong, T. a Springer, Mechanoenzymatic cleavage of the ultralarge vascular protein von Willebrand factor., Science. 324 (2009) 1330–4. doi:10.1126/science.1170905.

[16] B. Nieswandt, C. Brakebusch, W. Bergmeier, V. Schulte, D. Bouvard, R. Mokhtari-Nejad, et al., Glycoprotein VI but not alpha2beta1 integrin is essential for platelet interaction with collagen., EMBO J. 20 (2001) 2120–30. doi:10.1093/emboj/20.9.2120.

[17] K. Kremer, G.S. Grest, Dynamics of entangled linear polymer melts: A molecular-dynamics simulation, J. Chem. Phys. 92 (1990) 5057. doi:10.1063/1.458541.

[18] A. Alexander-katz, Toward Novel Polymer-Based Materials Inspired in Blood Clotting, Macromolecules. 47 (2014) 1503−1513. doi:dx.doi.org/10.1021/ma4007768.

[19] C.E. Sing, A. Alexander-Katz, Elongational flow induces the unfolding of von Willebrand factor at physiological flow rates., Biophys. J. 98 (2010) L35–7. doi:10.1016/j.bpj.2010.01.032.

[20] A. Alexander-Katz, M. Schneider, S. Schneider, A. Wixforth, R. Netz, Shear-Flow-Induced Unfolding of Polymeric Globules, Phys. Rev. Lett. 97 (2006) 138101. doi:10.1103/PhysRevLett.97.138101.

[21] S.W. Schneider, S. Nuschele, A. Wixforth, C. Gorzelanny, A. Alexander-Katz, R.R. Netz, et al., Shear-induced unfolding triggers adhesion of von Willebrand factor fibers., Proc. Natl. Acad. Sci. 104 (2007) 7899–903. doi:10.1073/pnas.0608422104.

[22] C.E. Sing, A. Alexander-katz, Force Spectroscopy of Self-Associating Homopolymers, Macromolecules. 45 (2012) 6704−6718. doi:dx.doi.org/10.1021/ma300785n.

[23] C.E. Sing, J.G. Selvidge, A. Alexander-Katz, Von Willlebrand adhesion to surfaces at high shear rates is controlled by long-lived bonds., Biophys. J. 105 (2013) 1475–81. doi:10.1016/j.bpj.2013.08.006.

[24] G.O. Ibáñez-García, P. Goldstein, S. Hanna, Brownian dynamics simulations of confined tethered polymers in shear flow: the effect of attractive surfaces., Eur. Phys. J. E. Soft Matter. 36 (2013) 56. doi:10.1140/epje/i2013-13056-5.

[25] P.T. Underhill, P.S. Doyle, On the coarse-graining of polymers into bead-spring chains, J. Nonnewton. Fluid Mech. 122 (2004) 3–31. doi:10.1016/j.jnnfm.2003.10.006.

[26] J. Kim, C.-Z. Zhang, X. Zhang, T. a Springer, A mechanically stabilized receptor-ligand flex-bond important in the vasculature., Nature. 466 (2010) 992–5. doi:10.1038/nature09295.

[27] S. Dutta, K.D. Dorfman, S. Kumar, Adsorption of single polymer molecules in shear flow near a planar wall Adsorption of single polymer molecules in shear flow near a planar wall, 034905 (2013). doi:10.1063/1.4773859.

[28] S. Dutta, K.D. Dorfman, S. Kumar, Dynamics of polymer adsorption from dilute solution in shear flow near a planar wall., J. Chem. Phys. 139 (2013) 174905. doi:10.1063/1.4773859.

[29] C. Sendner, R.R. Netz, Shear-induced repulsion of a semiflexible polymer from a wall, EPL (Europhysics Lett. 81 (2008) 54006. doi:10.1209/0295-5075/81/54006.

[30] Y. von Hansen, M. Hinczewski, R.R. Netz, Hydrodynamic screening near planar boundaries: effects on semiflexible polymer dynamics., J. Chem. Phys. 134 (2011) 235102. doi:10.1063/1.3593458.

[31] N. Hoda, S. Kumar, Brownian dynamics simulations of polyelectrolyte adsorption in shear flow with hydrodynamic interaction., J. Chem. Phys. 127 (2007) 234902. doi:10.1063/1.2806187.

[32] H. Ma, M.D. Graham, Theory of shear-induced migration in dilute polymer solutions near solid boundaries, Phys. Fluids. 17 (2005) 083103. doi:10.1063/1.2011367.

[33] a. Serr, C. Sendner, F. Müller, T.R. Einert, R.R. Netz, Single-polymer adsorption in shear: Flattening vs. hydrodynamic lift and surface potential corrugation effects, EPL (Europhysics Lett. 92 (2010) 38002. doi:10.1209/0295-5075/92/38002.

[34] O.B. Usta, J.E. Butler, A.J.C. Ladd, Flow-induced migration of polymers in dilute solution, Phys. Fluids. 18 (2006) 031703. doi:10.1063/1.2186591.

[35] C.E. Sing, a. Alexander-Katz, Non-monotonic hydrodynamic lift force on highly extended polymers near surfaces, EPL (Europhysics Lett. 95 (2011) 48001. doi:10.1209/0295-5075/95/48001.

[36] J.P. Hernández-Ortiz, H. Ma, J.J. de Pablo, M.D. Graham, Cross-stream-line migration in confined flowing polymer solutions: Theory and simulation, Phys. Fluids. 18 (2006) 123101. doi:10.1063/1.2397571.

[37] G. Bell, Models for the specific adhesion of cells to cells, Science (80-.). 200 (1978) 618–627. doi:10.1126/science.347575.

[38] E. Evans, K. Ritchie, Dynamic strength of molecular adhesion bonds., Biophys. J. 72 (1997) 1541–55. doi:10.1016/S0006-3495(97)78802-7.

[39] O.K. Dudko, G. Hummer, A. Szabo, Theory, analysis, and interpretation of single-molecule force spectroscopy experiments., Proc. Natl. Acad. Sci. U. S. A. 105 (2008) 15755–60. doi:10.1073/pnas.0806085105.

[40] N. Hoda, R.G. Larson, Brownian dynamics simulations of single polymer chains with and without self-entanglements in theta and good solvents under imposed flow fields, J. Rheol. (N. Y. N. Y). 54 (2010) 1061. doi:10.1122/1.3473925.

[41] C.-C. Hsieh, L. Li, R.G. Larson, Modeling hydrodynamic interaction in Brownian dynamics: simulations of extensional flows of dilute solutions of DNA and polystyrene, J. Nonnewton. Fluid Mech. 113 (2003) 147–191. doi:10.1016/S0377-0257(03)00107-1.

[42] D.L. Ermak, J.A. McCammon, Brownian dynamics with hydrodynamic interactions, J. Chem. Phys. 69 (1978) 1352. doi:10.1063/1.436761.

[43] R.M. Jendrejack, M.D. Graham, J.J. De Pablo, Hydrodynamic interactions in long chain polymers: Application of the Chebyshev polynomial approximation in stochastic simulations, J. Chem. Phys. 113 (2000) 2894. doi:10.1063/1.1305884.

[44] J. Rudisill, S. Fetsko, P. Cummings, Brownian-Dynamics Simulation of Chain Models for Dilute Polymer Solutions in Shear Flow, Comput. Polym. Sci. 3 (1993) 23–31.

[45] J.S. Hur, E.S.G. Shaqfeh, R.G. Larson, Brownian dynamics simulations of single DNA molecules in shear flow, J. Rheol. (N. Y. N. Y). 44 (2000) 713. doi:10.1122/1.551115.

[46] M. Chopra, R.G. Larson, Brownian dynamics simulations of isolated polymer molecules in shear flow near adsorbing and nonadsorbing surfaces, J. Rheol. (N. Y. N. Y). 46 (2002) 831. doi:10.1122/1.1485279.

[47] R.M. Jendrejack, J.J. De Pablo, M.D. Graham, Stochastic simulations of DNA in flow: Dynamics and the effects of hydrodynamic interactions, J. Chem. Phys. 116 (2002) 7752. doi:10.1063/1.1466831.

[48] R.G. Larson, The rheology of dilute solutions of flexible polymers: Progress and problems, J. Rheol. (N. Y. N. Y). 49 (2005) 1. doi:10.1122/1.1835336.

[49] M. Bercea, C. Ioan, S. Ioan, B.C. Simionescu, C.I. Simionescu, Ultrahigh molecular weight polymers in dilute solutions, 1999. doi:10.1016/S0079-6700(99)00007-6.

[50] S.L. Haberichter, M. Balistreri, P. Christopherson, P. Morateck, S. Gavazova, D.B. Bellissimo, et al., Assay of the von Willebrand factor (VWF) propeptide to identify patients with type 1 von Willebrand disease with decreased VWF survival., Blood. 108 (2006) 3344–51. doi:10.1182/blood-2006-04-015065.

[51] P.G. De Gennes, Coil-stretch transition of dilute flexible polymers under ultrahigh velocity gradients, J. Chem. Phys. 60 (1974) 5030. doi:10.1063/1.1681018.

[52] A. Buguin, Unwinding of Globular Polymers under Strong Flows, 9297 (1996) 4937–4943.

[53] P.S. Doyle, E.S.G. Shaqfeh, Dynamic simulation of freely-draining, flexible bead-rod chains: Start-up of extensional and shear flow, J. Nonnewton. Fluid Mech. 76 (1998) 43–78. doi:10.1016/S0377-0257(97)00112-2.

[54] J.S. Hur, E.S.G. Shaqfeh, R.G. Larson, Brownian dynamics simulations of single DNA molecules in shear flow, J. Rheol. (N. Y. N. Y). 44 (2000) 713–742. doi:doi:10.1122/1.551115.

[55] C.M. Schroeder, E.S.G. Shaqfeh, S. Chu, Effect of Hydrodynamic Interactions on DNA Dynamics in Extensional Flow: Simulation and Single Molecule Experiment, Macromolecules. 37 (2004) 9242–9256. doi:10.1021/ma049461l.

[56] D.E. Smith, Single-Polymer Dynamics in Steady Shear Flow, Science (80-.). 283 (1999) 1724–1727. doi:10.1126/science.283.5408.1724.

[57] D.E. Smith, Response of Flexible Polymers to a Sudden Elongational Flow, Science (80-.). 281 (1998) 1335–1340. doi:10.1126/science.281.5381.1335.

[58] R.G. Larson, H. Hu, D.E. Smith, S. Chu, Brownian dynamics simulations of a DNA molecule in an extensional flow field, J. Rheol. (N. Y. N. Y). 43 (1999) 267. doi:10.1122/1.550991.

[59] D. Petera, M. Muthukumar, Brownian dynamics simulation of bead–rod chains under shear with hydrodynamic interaction, J. Chem. Phys. 111 (1999) 7614. doi:10.1063/1.480087.

[60] C.E. Sing, A. Alexander-Katz, Designed molecular mechanics using self-associating polymers, Soft Matter. 8 (2012) 11871. doi:10.1039/c2sm26276b.

[61] D.M. Steppich, J.I. Angerer, J. Opfer, K. Sritharan, S.W. Schneider, S. Thalhammer, et al., Relaxation of ultralarge VWF bundles in a microfluidic-AFM

hybrid reactor., Biochem. Biophys. Res. Commun. 369 (2008) 507–12. doi:10.1016/j.bbrc.2008.02.062.

[62] T. Goerge, F. Kleinerüschkamp, A. Barg, E.-M. Schnaeker, V. Huck, M.F. Schneider, et al., Microfluidic reveals generation of platelet-strings on tumor-activated endothelium, Thromb. Haemost. (2007) 283–286. doi:10.1160/TH07-03-0163.

[63] T.T. Perkins, Single Polymer Dynamics in an Elongational Flow, Science (80-.). 276 (1997) 2016–2021. doi:10.1126/science.276.5321.2016.

[64] P. Szymczak, M. Cieplak, Hydrodynamic effects in proteins., J. Phys. Condens. Matter. 23 (2011) 033102. doi:10.1088/0953-8984/23/3/033102.

[65] M. Doi and S. F. Edwards, The theory of polymer dynamics, Oxford University Press Inc., 1986.

[66] M. Radtke, M. Radtke, R. Netz, Shear-induced dynamics of polymeric globules at adsorbing homogeneous and inhomogeneous surfaces., Eur. Phys. J. E. Soft Matter. 37 (2014) 20. doi:10.1140/epje/i2014-14020-7.

[67] A.O. Wenli Ouyang, Wei Wei, Xuanhong Cheng, Xiaohui Zhang, Edmund B. Webb III, Flow-induced conformational change of von Willebrand Factor multimer: results from a molecular mechanics informed model, J. Nonnewton. Fluid Mech. (2014).

[68] R. a Romijn, E. Westein, B. Bouma, M.E. Schiphorst, J.J. Sixma, P.J. Lenting, et al., Mapping the collagen-binding site in the von Willebrand factor-A3 domain., J. Biol. Chem. 278 (2003) 15035–9. doi:10.1074/jbc.M208977200.

[69] F. Li, J.L. Moake, L. V. McIntire, Characterization of von Willebrand Factor Interaction with Collagens in Real Time Using Surface Plasmon Resonance, Ann. Biomed. Eng. 30 (2002) 1107–1116. doi:10.1114/1.1521931.

[70] R.W. Farndale, J.J. Sixma, M.J. Barnes, P.G. de Groot, The role of collagen in thrombosis and hemostasis., J. Thromb. Haemost. 2 (2004) 561–73. doi:10.1111/j.1538-7836.2004.00665.x.

[71] M.D. Graham, Fluid dynamics of dissolved polymer molecules in confined geometries, Annu. Rev. Fluid Mech. 43 (2011) 273–298. doi:DOI: 10.1146/annurev-fluid-121108-145523.

[72] R.M. Jendrejack, E.T. Dimalanta, D.C. Schwartz, M.D. Graham, J.J. De Pablo, DNA dynamics in a microchannel., Phys. Rev. Lett. 91 (2003) 038102. doi:10.1103/PhysRevLett.91.038102.

[73] R.M. Jendrejack, D.C. Schwartz, M.D. Graham, J.J. De Pablo, Effect of confinement on DNA dynamics in microfluidic devices, J. Chem. Phys. 119 (2003) 1165. doi:10.1063/1.1575200.

[74] R.M. Jendrejack, D.C. Schwartz, J.J. de Pablo, M.D. Graham, Shear-induced migration in flowing polymer solutions: simulation of long-chain DNA in microchannels [corrected]., J. Chem. Phys. 120 (2004) 2513–29. doi:10.1063/1.1637331.

[75] J.P. Hernández-Ortiz, J.J. de Pablo, M.D. Graham, N log N method for hydrodynamic interactions of confined polymer systems: Brownian dynamics., J. Chem. Phys. 125 (2006) 164906. doi:10.1063/1.2358344.

[76] R. Khare, M. Graham, J. de Pablo, Cross-Stream Migration of Flexible Molecules in a Nanochannel, Phys. Rev. Lett. 96 (2006) 224505. doi:10.1103/PhysRevLett.96.224505.

[77] T. a Springer, Biology and physics of von Willebrand factor concatamers., J. Thromb. Haemost. 9 Suppl 1 (2011) 130–43. doi:10.1111/j.1538-7836.2011.04320.x.

[78] Z.M. Ruggeri, J.N. Orje, R. Habermann, A.B. Federici, A.J. Reininger, Activation-independent platelet adhesion and aggregation under elevated shear stress., Blood. 108 (2006) 1903–10. doi:10.1182/blood-2006-04-011551.

W. Wayne Ouyang

212 Apt 10 DUH Drive, Bethlehem PA 18015
(C) (484) 767-8123 (E) ouyangwenli@gmail.com

Education

2014 **Lehigh University** - Bethlehem, PA, USA
Ph.D.: Mechanical Engineering
3.72 GPA
Thesis "Characteristics of von Willebrand Factor multimer in blood clotting".
Research on steady/unsteady flow and heat transfer across multiple length and time scales.

2012 **Lehigh University** - Bethlehem, PA, USA
Master of Science: Mechanical Engineering
3.68 GPA
Thesis "Simulation of single polymer chains with influences of solid walls under imposed flow fields".

2010 **Huazhong University of Sci & Tech** Wuhan, China
Bachelor of Science: Mechanical Engineering

Professional Experience

02/2013 - 11/2013 **Hunsicker Emissions LLC** - Earlington, PA
Product Engineer
- Innovated and designed new Diesel Particulate Filter cleaning system using Catalyst Wash and Baking.
- The new DPF Cleaning system greatly decreased downtime from 1 day to several hours, which make next day turnaround time possible.

02/2013 - 11/2013 **Industrial Assessment center, Lehigh University & U.S. DOE** - Behtlehem, PA
Energy Auditor
- Examine the manufacturing process, collect system data, and analyze energy efficiency of industrial boilers, refrigeration, lighting, and air compressor.
- Provide assessment reports for manufacturers to reduce energy consumption minimize waste and increase productivity.

11/2010 - 08/2011 **Lehigh University** - Bethlehem, PA
Research Assistant
- research on mechanics of composite materials and structures.
- build a high-speed boat made of composite-steel hybrid materials.

06/2009 - 10/2009 **Wuchang Shipbuilding Company Ltd** - Wuhan, China
Engineering Assistant
- Design propellers for cargo ships using AutoCAD and ProE.
- Analysis mechanical properties of propellers using ANSYS and SolidWorks.

06/2008 - 10/2008 **Dongfeng Motor Inc** - Wuhan, China
Job Foreman
- Supervised four workers at all stages of automobile assembly process.
- Gained enough knowledge of how assembly lines work and methods to operate comprehensive engineering machinaries.

Skills

C/C++, Fortran, Labview, Matlab, ABAQUS, Optimization, Project Management